Article

Inhibition of LTβR signalling activates WNT-induced regeneration in lung

Thomas M. Conlon[1,21], Gerrit John-Schuster[1,21], Danijela Heide[2], Dominik Pfister[2], Mareike Lehmann[3], Yan Hu[4], Zeynep Ertüz[1], Martin A. Lopez[5], Meshal Ansari[1,6], Maximilian Strunz[1], Christoph Mayr[1], Ilias Angelidis[1], Chiara Ciminieri[4,7], Rita Costa[3], Marlene Sophia Kohlhepp[8], Adrien Guillot[8], Gizem Günes[1], Aicha Jeridi[1], Maja C. Funk[9], Giorgi Beroshvili[1], Sandra Prokosch[2], Jenny Hetzer[2], Stijn E. Verleden[10], Hani Alsafadi[3,11], Michael Lindner[12,13], Gerald Burgstaller[1], Lore Becker[14], Martin Irmler[14], Michael Dudek[15], Jakob Janzen[2,16], Eric Goffin[17], Reinoud Gosens[7], Percy Knolle[15], Bernard Pirotte[17], Tobias Stoeger[1], Johannes Beckers[14,18,19], Darcy Wagner[3,11], Indrabahadur Singh[16], Fabian J. Theis[6], Martin Hrabé de Angelis[14,18,19], Tracy O'Connor[2], Frank Tacke[8], Michael Boutros[9,20], Emmanuel Dejardin[5], Oliver Eickelberg[4], Herbert B. Schiller[1], Melanie Königshoff[3,4], Mathias Heikenwalder[2,21 ✉] & Ali Önder Yildirim[1,21 ✉]

Lymphotoxin β-receptor (LTβR) signalling promotes lymphoid neogenesis and the development of tertiary lymphoid structures[1,2], which are associated with severe chronic inflammatory diseases that span several organ systems[3–6]. How LTβR signalling drives chronic tissue damage particularly in the lung, the mechanism(s) that regulate this process, and whether LTβR blockade might be of therapeutic value have remained unclear. Here we demonstrate increased expression of LTβR ligands in adaptive and innate immune cells, enhanced non-canonical NF-κB signalling, and enriched LTβR target gene expression in lung epithelial cells from patients with smoking-associated chronic obstructive pulmonary disease (COPD) and from mice chronically exposed to cigarette smoke. Therapeutic inhibition of LTβR signalling in young and aged mice disrupted smoking-related inducible bronchus-associated lymphoid tissue, induced regeneration of lung tissue, and reverted airway fibrosis and systemic muscle wasting. Mechanistically, blockade of LTβR signalling dampened epithelial non-canonical activation of NF-κB, reduced TGFβ signalling in airways, and induced regeneration by preventing epithelial cell death and activating WNT/β-catenin signalling in alveolar epithelial progenitor cells. These findings suggest that inhibition of LTβR signalling represents a viable therapeutic option that combines prevention of tertiary lymphoid structures[1] and inhibition of apoptosis with tissue-regenerative strategies.

Endogenous regenerative mechanisms of the lung are severely compromised in chronic obstructive pulmonary disease (COPD), the third leading cause of death worldwide[7] with limited therapeutic options[8]. Consequently, the identification and therapeutic use of endogenous regenerative mechanisms is an important paradigm shift in our understanding and potential treatment of COPD[9]. Notably, immune cells that infiltrate the lung in COPD are organized into tertiary lymphoid structures known as inducible bronchus-associated lymphoid tissue (iBALT), which are observed during destruction of lung tissue (emphysema) in both humans[3,10–12] and mice[13,14]. Formation of iBALT requires the interaction of the lymphotoxin β-receptor (LTβR) on stromal organizer cells with TNF superfamily members lymphotoxin-α (LTα) and LTβ[1,2], expressed by activated lymphocytes during chronic inflammation[15,16]. Stimulation of LTβR subsequently triggers downstream non-canonical NF-κB signalling via the activation of NF-κB-inducing kinase (NIK)[17,18]. However, the role of LTβR signalling in the development of lung tissue injury remains unknown.

Analysis of lung samples from patients with COPD revealed increased expression of signalling molecules *LTA*, *TNFSF14* (also known as *LIGHT*) and *TNF*, and downstream chemokines *CCL2*, *CXCL8* and *CXCL13* (Fig. 1a), mediated through increased nuclear translocation of NF-κB-associated transcription factors RELA and RELB in lung epithelium (Extended Data Fig. 1a, b). To validate these findings, we performed gene set enrichment analysis (GSEA) of lung transcriptomic data from patients with COPD (GSE47460 and GSE37768). Analysis showed the enrichment of both LTβR and TNF receptor signalling pathways, together with enhanced IKK-dependent canonical and NIK-dependent non-canonical NF-κB signalling in COPD lungs (Extended Data Fig. 1c, d). Notably, similar enrichment was also found in peripheral blood mononuclear cells (PBMCs) from patients with COPD (GSE56768) (Extended Data Fig. 1e). Similarly, mice chronically exposed to cigarette smoke for six months displayed increased mRNA expression of *Lta*, *Tnf*, *Ccl2* and *Cxcl13* in lung tissue (Extended Data Fig. 1f). Furthermore, GSEA of
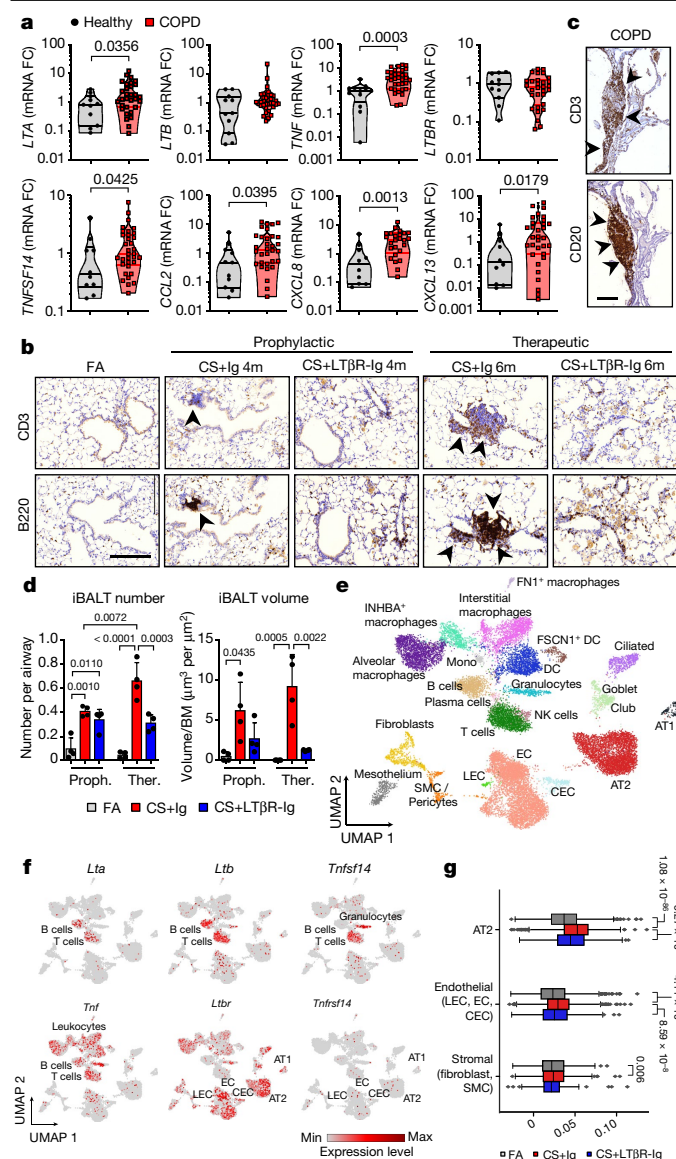
Fig. 1 | LTβR-signalling is activated in COPD and inhibition disrupts iBALT in the lungs of mice exposed to cigarette smoke. a, mRNA expression of genes determined by qPCR in lung core biopsies from healthy participants ($n = 11$) and patients with COPD ($n = 32$). FC, fold change. **b**, Representative images of immunohistochemical analysis for B220^{+} B cells and CD3^{+} T cells (brown signal, arrows, nuclei counterstained with haematoxylin) in lung sections from B6 mice exposed to filtered air (FA) or cigarette smoke (CS) for 4 or 6 months, plus LTβR–Ig or control Ig prophylactically from 2 to 4 months (CS + LTβR-Ig 4m) and therapeutically from 4 to 6 months (CS + LTβR-Ig 6 m) ($n = 4$ mice per group, repeated twice). See Extended Data Fig. 1i. Scale bar, 200 µm. **c**, Representative lung sections from patients with COPD stained for CD20^{+} B cells and CD3^{+} T cells (brown signal, arrows, nuclei counterstained with haematoxylin; $n = 4$). Scale bar, 200 µm. **d**, Quantification of lung iBALT from mice described in **b**, as mean iBALT number per airway and volume of iBALT normalized to surface area of airway basement membrane (BM). Data are mean ± s.d. ($n = 4$ mice per group, repeated twice). Proph., prophylactic; Ther., therapeutic. **e**–**g**, Cells from whole lung suspensions of B6 mice exposed to filtered air ($n = 3$) or cigarette smoke for 6 months, plus LTβR–Ig ($n = 5$) or control Ig ($n = 5$) therapeutically, were analysed at 6 months by scRNA-seq (Drop-Seq). **e**, UMAP of scRNA-seq profiles (dots) coloured by cell type. DC, dendritic cells; EC, endothelial cells; CEC, circulating endothelial cells; LEC, lymphatic endothelial cells; NK cells, natural killer cells; SMC, smooth muscle cells. **f**, Uniform manifold approximation and projection (UMAP) plots showing expression of genes indicated in scRNA-seq profiles. **g**, Box and whiskers plot (box edges denote 25th–75th percentile, horizontal lines denotes median and whiskers represent ±1.5 times the interquartile range (IQR)) showing relative score for positive regulation of NIK (non-canonical) NF-κB signalling pathway (GO:1901224) in indicated cells. P values were determined by one-sided Mann–Whitney test (**a**), one-way analysis of variance (ANOVA) with multiple comparisons Bonferroni test (**d**) or Wilcoxon rank-sum test on normalized, log-transformed count values and corrected with Benjamini–Hochberg (**g**).

our transcriptomics dataset (GSE52509) demonstrated enrichment of LTβR, TNFR and both canonical and non-canonical NF-κB signalling pathways in lungs of mice exposed to cigarette smoke (Extended Data Fig. 1g), accompanied by increased protein levels of RELB, p100 and its cleaved product p52 (Extended Data Fig. 1h). Next, we analysed whether inhibition of LTβR signalling might impair iBALT formation by applying distinct treatment strategies using a LTβR–Ig fusion protein[19,20] (Extended Data Fig. 1i). Exposure to cigarette smoke resulted in the development of iBALT, composed predominantly of organized B cell and T cell clusters as early as 4 months (Fig. 1b), reminiscent to that observed in patients with COPD (Fig. 1c). LTβR–Ig treatment, in the presence of cigarette smoke, led to considerably reduced iBALT formation with dispersed immune cells (Fig. 1b, d, Extended Data Fig. 1j), accompanied by a reduction of the LTβR signalling downstream targets *Cxcl13* and *Ccl19* (Extended Data Fig. 1k). The effect of LTβR–Ig treatment was specific to a reduction in iBALT incidence, as multicolour flow cytometric analysis of adaptive immune cells revealed no significant effect on their abundance or activation status (Extended Data Fig. 2a–c). Furthermore, macrophages were not significantly reduced in the lungs of mice exposed to cigarette smoke plus LTβR–Ig compared with those exposed to cigarette smoke plus Ig (Extended Data Fig. 2d, e). Multiplex immunofluorescence analysis suggested only subtle differences in myeloid populations after LTβR–Ig treatment, a trend

towards reduction was found in iNOS[+] IBA1^{+} macrophages after therapeutic LTβR–Ig treatment (Extended Data Fig. 2f, g). Multicolour flow cytometric analysis of interstitial macrophages in particular showed that both the abundance and the expression of inflammatory CD86^{+} and immune-modulatory CD206^{+} macrophage populations induced by cigarette smoke exposure were not reduced after treatment with LTβR–Ig (Extended Data Fig. 2h–l).

To further determine the cellular and molecular consequences of LTβR inhibition, we investigated single-cell RNA sequencing (scRNA-seq) together with bulk transcriptomic and proteomic analyses. We grouped single-cell transcriptomes from whole mouse lung tissue into 24 cell identities and observed cell type-specific changes after cigarette smoke exposure and LTβR–Ig treatment (Fig. 1e, Extended Data Fig. 3a–d). Expression of *Lta* and *Ltb* localized mainly to B and T cells, *Tnfsf14* (an alternative LTβR ligand) localized to T cells and granulocytes, whereas *Tnf* was expressed by all leucocytes in the lung (Fig. 1f). Expression of *Ltb* but not *Tnf* was reduced after LTβR–Ig treatment (Extended Data Fig. 3d), which was validated by cellular localization with in situ hybridization and immunohistochemistry (Extended Data Fig. 4a–e). Concomitant with disease progression cigarette smoke strongly induced a positive regulation of NIK-dependent non-canonical NF-κB signalling in alveolar epithelial type 2 (AT2) cells, which was significantly reduced after LTβR–Ig treatment (Fig. 1g, Extended Data Fig. 3e–g). We found high levels of *Ltbr* mRNA expression in AT2 cells (Fig. 1f), which indicates that NIK-dependent NF-κB-signalling in AT2 cells can be triggered by LTβR activation. By contrast, expression of *Hvem* (also known as *Tnfrsf14*), an additional receptor for *Tnfsf14*, was hardly detectable in lung tissue (Fig. 1f).

Bulk level principle component analyses revealed a distinct change in the lung transcriptome (Extended Data Fig. 5a) and proteome (Extended Data Fig. 5b) of mice treated with cigarette smoke and either LTβR–Ig or Ig, with non-canonical NF-κB targets *Cxcl13* and

Ccl19 to be among the most downregulated after treatment with LTβR–Ig (Extended Data Fig. 5c). GSEA confirmed NIK-associated non-canonical NF-κB signalling to be reversed by LTβR–Ig treatment at transcriptomic and proteomic level (Extended Data Fig. 5d–f). LTβR–Ig treatment reduced cigarette-smoke-induced increases in nuclear translocation of RELB in lung epithelial cells (Extended Data Fig. 5g, h). By contrast, nuclear translocation of RELA in lung epithelial cells was not affected by LTβR–Ig treatment (Extended Data Fig. 5i, j), along with canonical NF-κB regulated genes *Ccl2*, *Ccl3*, *Cxcl1* and *Tnf* (Extended Data Fig. 5k). Moreover, we demonstrated the clinical relevance of these findings by modelling COPD inflammation in human precision-cut lung slices (PCLS) ex vivo[21,22]. Lipopolysaccharide (LPS) stimulation resulted in increased expression of *LTA*, *TNF* and *CXCL13*, and treatment with human LTβR–Ig reversed the increase in *LTA* and *CXCL13* but not canonical NF-κB-regulated *TNF* (Extended Data Fig. 5l). These data indicate that disruption of the LTβR signalling pathway reverses cigarette-smoke-induced iBALT formation and modulates non-canonical NF-κB signalling in lung tissue.

We next assessed whether reduction in LTβR signalling and diminution of iBALT affected cigarette-smoke-associated lung pathogenesis. Quantitative morphological analyses of lung tissue damage (Fig. 2a) for airspace enlargement and alveolar surface density revealed that cigarette-smoke-induced emphysema was prevented by prophylactic LTβR–Ig treatment (Fig. 2b). Therapeutic treatment starting from 4 months, a time point at which airspace damage was already fully established in mice[14], led to full restoration of lung tissue—even under concomitant exposure to cigarette smoke (Fig. 2b). Furthermore, quantification of collagen deposition around the airways, particularly the accumulation of collagen I, revealed that LTβR–Ig treatment is protective in the prophylactic group (Fig. 2c, d, Extended Data Fig. 6a–c) and induced regression of cigarette-smoke-mediated airway-remodelling in the therapeutic group (Fig. 2c, d, Extended Data Fig. 6a–c). Airway-remodelling processes are mediated via TGFβ signalling, propagated by phosphorylation of the receptor-regulated SMAD proteins[23]. In line, staining for phosphorylated SMAD2 revealed high levels in airway epithelial cells of cigarette-smoke-exposed mice, which was strongly reduced after LTβR–Ig (Extended Data Fig. 6d). Notably, levels of active TGFβ in the bronchoalveolar lavage (BAL) fluid increased after cigarette-smoke exposure (Fig. 2e), and was reversed after therapeutic LTβR–Ig treatment.

COPD is further characterized by comorbidities, most prominently muscle wasting[24]. Thus, we analysed the systemic responses to therapeutic LTβR–Ig treatment in mice. Transcriptomic analysis of the gastrocnemius muscle suggested that cigarette-smoke-induced modulation of *Ppargc1a* and *Mcat*[25,26] was reversed after LTβR–Ig treatment (Extended Data Fig. 6e). Furthermore, a functional 4-paw muscle strength test revealed a significant deficit in mice after 6 months of exposure to cigarette smoke, and this could be fully reversed after LTβR–Ig treatment (Extended Data Fig. 6f).

We have previously shown that aged mice are predisposed to earlier development of cigarette-smoke-induced airway remodelling and emphysema via iBALT driven immune-ageing[27]. To determine whether findings of this study are age-independent, we exposed aged mice (12 months) to cigarette smoke for 4 months, combined with therapeutic LTβR–Ig treatment under cigarette smoke for 2 months (Extended Data Fig. 6g). Cigarette smoke-induced iBALT, emphysema and airway remodelling were also prevented by LTβR–-Ig treatment in aged mice (Fig. 2f, g, Extended Data Fig. 6h), which indicates that our findings are age-independent.

We next asked whether the therapeutic effect of LTβR–Ig on chronic smoking-associated lung tissue is directly related to the blocking of LTβR signalling. To address this, we examined the effect of LTβR–Ig treatment in the porcine pancreatic elastase (PPE)-induced emphysema model (Extended Data Fig. 7a), a LTβR-signalling and iBALT-independent mouse model (Extended Data Fig. 7b, c). We observed no detectable
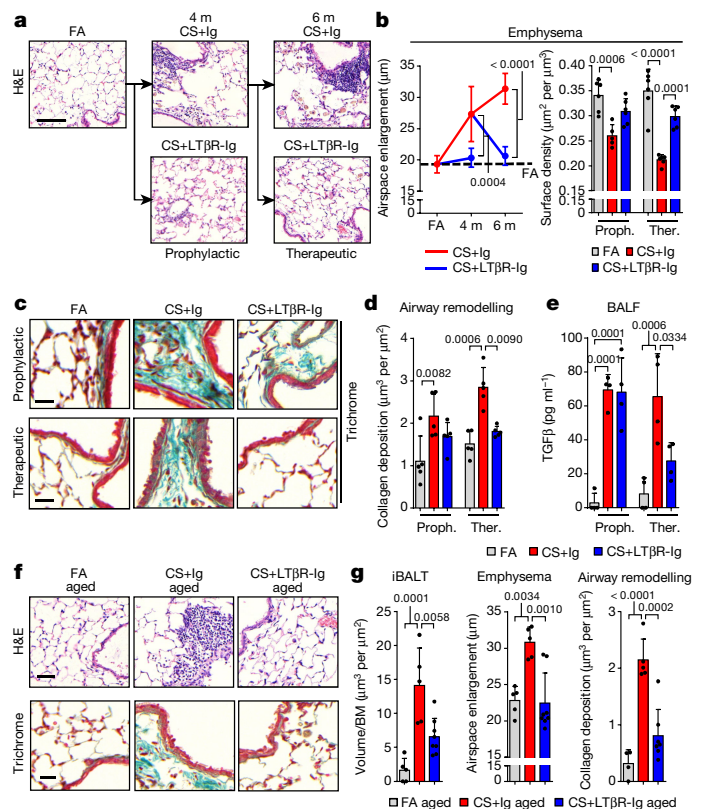
Fig. 2 | LTβR–Ig reverses emphysema in young and aged mice chronically exposed to cigarette smoke. a, Representative images of haematoxylin and eosin (H&E)-stained lung sections from B6 mice exposed to filtered air or cigarette smoke for 4 or 6 months, plus LTβR–Ig or control Ig prophylactically from 2 to 4 months, analysed at 4 months, and therapeutically from 4 to 6 months, analysed at 6 months (*n* = 6 mice FA, 5 mice CS+Ig, 6 mice CS+LTβR–Ig groups, repeated twice). Scale bar, 100 μm. See Extended Data Fig. 1i. **b**, Quantification of airspace enlargement as mean chord length and alveolar surface area in lung sections from mice in **a** (*n* = 6 mice FA, 5 mice CS+Ig, 6 mice CS+LTβR–Ig groups, repeated twice. **c**, Representative images of lung sections stained with Masson's Trichrome from mice in **a** (*n* = 5 mice FA, 5 mice CS+Ig, 5 mice CS+LTβR–Ig groups, repeated twice). Scale bar, 25 μm. **d**, Quantification of airway collagen deposition normalized to surface area of airway basement membrane from sections in **c** (*n* = 5 mice FA, 5 mice CS+Ig, 5 mice CS+LTβR–Ig groups, repeated twice). **e**, Levels of TGFβ determined by ELISA in BAL fluid of mice described in **a** (*n* = 4 mice FA, 4 mice CS+Ig, 4 mice CS+LTβR–Ig groups, repeated twice). **f**, Representative images of H&E and Masson's Trichrome-stained lung sections from 12-month-old B6 mice exposed to filtered air or cigarette smoke for 4 months, plus LTβR–Ig or control Ig from 2 to 4 months and analysed at 4 months (*n* = 5 mice FA, 5 mice CS+Ig, 8 mice CS+LTβR–Ig groups, repeated twice). See Extended Data Fig. 6g. **g**, Quantification of lung iBALT as volume of iBALT normalized to surface area of airway basement membrane, quantification of airspace enlargement as mean chord length, from H&E sections in **f**, and quantification of airway collagen deposition normalized to surface area of airway basement membrane from Masson's Trichrome sections in **f** (*n* = 5 mice FA, 5 mice CS+Ig, 8 mice CS+LTβR–Ig groups, repeated twice). Data are mean ± s.d. *P* values determined by one-way ANOVA multiple comparisons Bonferroni test.

increase in mRNA expression of *Lta*, *Ltb* or *Tnfsf14* (Extended Data Fig. 7b, e) or PPE-induced nuclear localization of RELA and RELB in lung epithelial cells (Extended Data Fig. 7f). In contrast to the cigarette smoke model, the PPE model displayed lower amounts of lymphocytes in BAL fluid (Extended Data Fig. 7d). Histological analyses of lung sections (Extended Data Fig. 7g, h) and analysis of lung function (Extended Data Fig. 7i, j) showed that LTβR–Ig treatment could not reverse elastase-induced emphysema. This confirmed that LTβR-signal
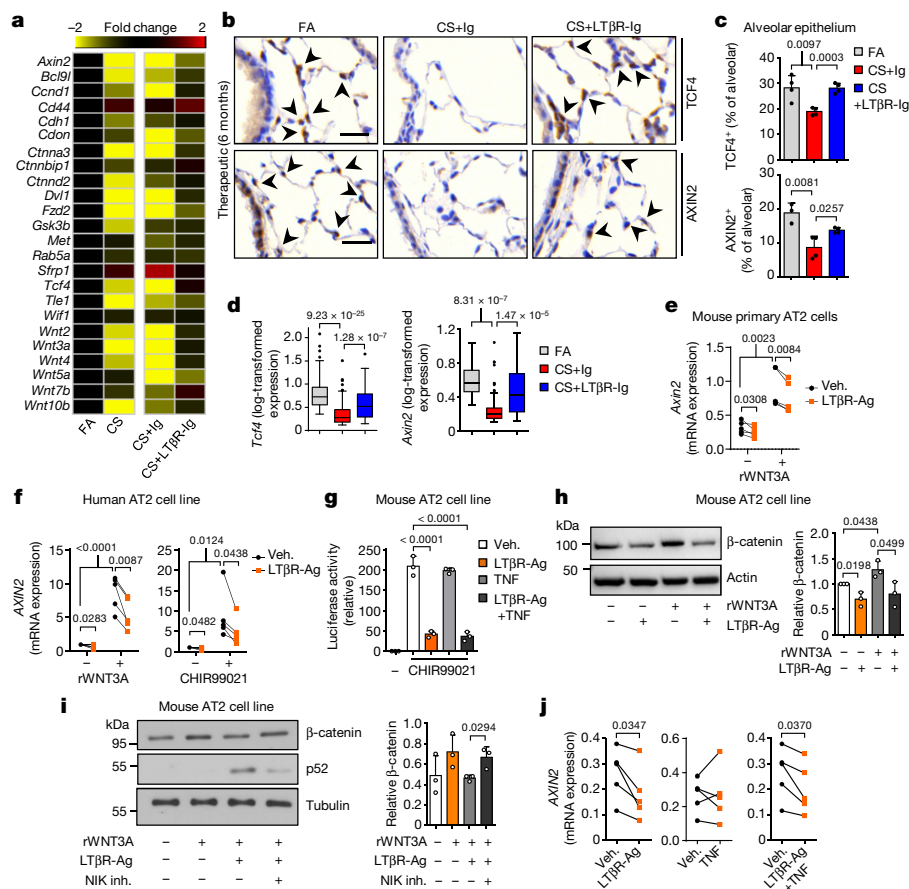
Fig. 3 | Blocking LTβR induces WNT/β-catenin signalling in alveolar epithelial cells. a, Heat map of mRNA abundance of WNT signalling pathway genes determined by quantitative PCR with reverse transcription (RT–qPCR) from lungs of mice indicated at 6 months. **b**, Representative images of immunohistochemical analysis for TCF4 and AXIN2 in lung sections from B6 mice treated as indicated ($n = 4$ mice per group; brown signal, arrows, nuclei counterstained with haematoxylin). Scale bar, 25 μm. **c**, Quantification of alveolar epithelial cells positive for TCF4 and AXIN2 from **b**. **d**, Normalized log-transformed expression levels of *Tcf4* and *Axin2* in AT2 cells following scRNA-seq analysis of cells from whole lung suspensions of B6 mice exposed to filtered air (FA, $n = 3$) or cigarette smoke (CS) for 6 months, plus LTβR–Ig ($n = 5$) or control Ig ($n = 5$) therapeutically. **e**, mRNA expression levels of *Axin2* relative to *Hprt*, in primary mouse AT2 cells with LTβR-Ag ($2 \, \mu g \, ml^{-1}$) for 24 h with or without WNT3A ($100 \, ng \, ml^{-1}$) ($n = 5$ independent experiments). **f**, mRNA expression levels of *AXIN2* relative to *HPRT* (normalized to vehicle (Veh.)) in A549 (human AT2) cell line with human LTβR-Ag ($0.5 \, \mu g \, ml^{-1}$) for 24h with or without WNT3A ($100 \, ng \, ml^{-1}$) and GSK-3β inhibitor (CHIR99021, $1 \, \mu M$) ($n = 5$ independent experiments). **g**, WNT/β-catenin luciferase reporter activity in

the mouse AT2 cell line MLE12, activated with CHIR99021 ($1 \, \mu M$) with or without LTβR-Ag ($2 \, \mu g \, ml^{-1}$) or rTNF ($1 \, ng \, ml^{-1}$) for 24 h ($n = 3$, representative of 5 independent experiments). **h**, Western blot analysis for β-catenin in MLE12 cells with LTβR-Ag ($2 \, \mu g \, ml^{-1}$) for 24 h with or without rWNT3A ($100 \, ng \, ml^{-1}$). Quantification relative to actin ($n = 3$ independent experiments). For gel source data, see Supplementary Fig. 1. **i**, Western blot analysis for β-catenin and p52 in MLE12 cells with rWNT3A ($200 \, ng \, ml^{-1}$) and LTβR-Ag ($2 \, \mu g \, ml^{-1}$) for 30 h after 2 h pre-treatment with NIK kinase specific inhibitor (CMP1, $1 \, \mu M$). Quantification relative to tubulin ($n = 3$ independent experiments). For gel source data, see Supplementary Fig. 1. **j**, mRNA expression level of *AXIN2* relative to *HPRT*, in ex vivo human precision-cut lung slices stimulated for 24 h with rTNF ($20 \, ng \, ml^{-1}$) or human LTβR-Ag ($2 \, \mu g \, ml^{-1}$) ($n = 5$ slices from individual lungs). Data are mean ± s.d. (**c**, **g–i**), box and whiskers plots (box edges 25th–75th percentile, median line indicated and whiskers representing ±1.5 × IQR) (**d**), individual lungs (**e**, **j**), or individual experiments (**f**). *P* values determined by one-way ANOVA multiple comparisons Bonferroni test (**g**), two-sided Wilcoxon rank-sum test corrected with Benjamini–Hochberg (**d**), paired Student's two-tailed *t*-test (**e**, **f**, **j**), or Student's two-tailed *t*-test (**c**, **h**, **i**).

---

blockade is specifically relevant to iBALT-mediated, LTβR-signalling induced emphysema.

Next, we aimed at identifying how blocking LTβR signalling promotes endogenous lung regeneration in emphysema. NIK is necessary for the activation of caspase-8 and subsequent downstream activation of caspase-3, by promoting the assembly of the RIP1/FADD/caspase-8 death complex after TNFR1 and lymphotoxin stimulation[28]. Indeed, lung tissue sections from patients with COPD demonstrated increased cleaved caspase-3-positive alveolar epithelial cells (Extended Data Fig. 8a, b). Furthermore, GSEA of lung tissue from patients with COPD and mice exposed to cigarette smoke showed enrichment of the apoptotic signature, which was reversed by LTβR–Ig treatment in mice (Extended Data Fig. 8c, d), and in AT2 epithelial cells as identified

by scRNA-seq (Extended Data Fig. 8e). This was confirmed by GSEA of whole lung proteome (Extended Data Fig. 8f, g), and by cleaved caspase-3 in both lung sections and lung lysates (Extended Data Fig. 8h, i). To examine LTβR signalling in lung epithelial apoptosis, we stimulated mouse lung epithelial cells with a LTβR agonistic antibody (LTβR-Ag) and/or TNF (Extended Data Fig. 8j, k). Maximum cell death was achieved by a combination of both, which was significantly reduced by inhibition of RIP1 kinase with necrostatin-1 (Extended Data Fig. 8j, k). We validated that cell death was caspase-dependent, as it was completely abrogated in the presence of the pan-caspase inhibitor Z-Val-Ala-DL-Asp-fluoromethylketone (z-VAD-FMK) (Extended Data Fig. 8l). Notably, blocking apoptosis enabled partial wound regeneration in vitro (Extended Data Fig. 8m, n).
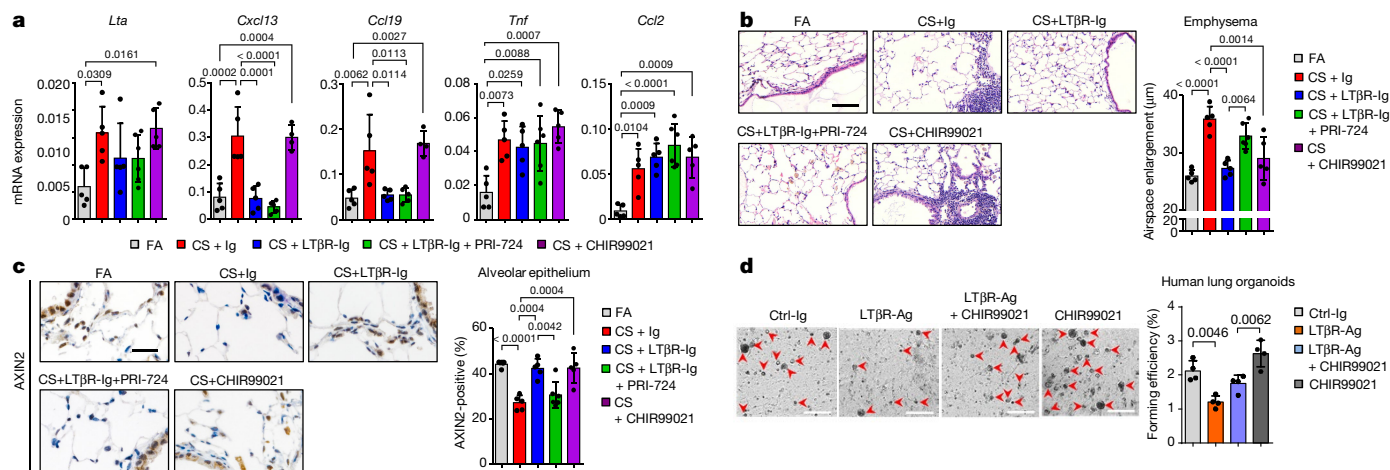
Fig. 4 | Blocking WNT/β-catenin signalling reverses LTβR–Ig-induced regeneration. a–c, B6 mice were exposed to filtered air ($n = 5$) or cigarette smoke for 6 months plus control Ig ($n = 5$), LTβR–Ig (80 μg intraperitoneally, weekly, $n = 5$), LTβR–Ig plus β-catenin/CBP inhibitor PRI-724 (0.6 mg intraperitoneally, twice weekly, $n = 6$) or CHIR99021 (0.75 mg intraperitoneally, weekly, $n = 5$) from 4 to 6 months, and analysed at 6 months. See Extended Data Fig. 10a. **a**, Lung mRNA expression levels of genes relative to *Hprt* determined by qPCR. **b**, Representative images of H&E-stained lung sections, and quantification of airspace enlargement as mean chord length. Scale bar, 100 μm. **c**, Representative images of immunohistochemical analysis for AXIN2 in lung sections (brown signal, nuclei counterstained with haematoxylin), and quantification of alveolar epithelial cells positive for AXIN2. Scale bar, 50 μm. **d**, Representative images and quantification of lung organoids from primary human AT2 cells cultured for 14 days with or without human LTβR-Ag (2 μg ml⁻¹) and CHIR99021 (2 μM) ($n = 2$ replicates from 2 separate donors). Scale bar, 500 μm. See Extended Data Fig. 10e. Data are mean ± s.d. *P* values determined by one-way ANOVA multiple comparisons Bonferroni test (**a–d**).

However, the mechanisms by which blocking LTβR signalling promotes lung regeneration (Fig. 2b, g) remained unclear. The developmental WNT/β-catenin signalling pathway is essential for lung development and homeostasis of progenitor AT2 stem-cell function[29,30]. Our previous studies have demonstrated reduced WNT/β-catenin signalling in COPD and have indicated that activation of WNT/β-catenin signalling can induce lung repair[21,31]. In agreement, GSEA analysis of lung tissue transcriptomics (GSE47460) confirmed dampened WNT/β-catenin signalling and reduced β-catenin/TCF transcription factor complex assembly in lung tissue from patients with COPD, resulting in reduced AXIN2 expression (Extended Data Fig. 9a, b). A similar pattern was found in lungs of mice exposed to cigarette smoke plus Ig control (Fig. 3a, Extended Data Fig. 9a). Notably, these transcriptional changes were significantly reversed by treatment with LTβR–Ig (Fig. 3a, Extended Data Fig. 9a): by combining immunostainings for the WNT/β-catenin target genes TCF4 and AXIN2 (Fig. 3b, c), and scRNA-seq analysis (Fig. 3d), we found that expression of these genes is specifically reduced in AT2 cells after cigarette smoke exposure and is therapeutically restored by LTβR–Ig treatment (Fig. 3b–d).

To establish a direct link between LTβR and WNT/β-catenin signalling, primary AT2 cells and stable human and mouse cell lines were treated with LTβR agonists, which led to a downregulation of the key WNT/β-catenin target genes *Axin2*, *Nkd1*, *Lgr5* and *Tcf4* (Fig. 3e, f, Extended Data Fig. 9c, d). This was reversed by inhibition of NF-κB signalling (Extended Data Fig. 9e, f). Notably, ligand-independent β-catenin transcriptional reporter activity induced by inhibition of GSK-3β was abrogated by LTβR agonization (Fig. 3g, Extended Data Fig. 9g), thus suggesting intracellular signal modification downstream of the β-catenin destruction complex. Indeed, enhanced β-catenin degradation was observed upon LTβR agonization (Fig. 3h), which was reversed after proteasome inhibition with bortezomib (Extended Data Fig. 9h). Targeting AT2 cells with the NIK kinase-specific inhibitor CMP1[32], reversed LTβR-Ag-induced degradation of β-catenin (Fig. 3i), further confirming that LTβR-activation decreased WNT/β-catenin signalling via NIK-dependent non-canonical NF-κB signalling. Furthermore, in a LTβR-signalling independent PPE-induced emphysema mouse model (Extended Data Fig. 7e, f) that also exhibits reduced WNT/β-catenin signalling[31], LTβR–Ig treatment neither reversed emphysema (Extended Data Fig. 7g, h), nor restored WNT/β-catenin signalling (Extended Data Fig. 9k–m).

Notably, both *AXIN2* and *TCF4* expression were also suppressed in ex vivo human PCLS stimulated with LTβR agonist (Fig. 3j, Extended Data Fig. 9i). Of note, non-canonical NF-κB signalling induced by the alternative LTβR ligand TNFSF14, also reduced β-catenin levels (Extended Data Fig. 9j).

Finally, to test the hypothesis that LTβR–Ig treatment induces lung tissue regeneration after chronic cigarette smoke exposure via endogenous WNT/β-catenin signalling in vivo, mice were treated with (1) LTβR–Ig; (2) LTβR–Ig and the β-catenin/CBP inhibitor PRI-724[33]; and (3) CHIR99021, a WNT/β-catenin activator[34] (Extended Data Fig. 10a). Similar to previous results (Fig. 1b, d, Extended Data Fig. 1k), LTβR–Ig treatment reduced the expression of *Lta*, *Cxcl13* and *Ccl19* (Fig. 4a) and reversed iBALT formation (Extended Data Fig. 10c). *Ltb*, *Tnfsf14* and *Ltbr* levels (Extended Data Fig. 10b) as well as canonical NF-κB-signalling regulated *Tnf* and *Ccl2* (Fig. 4a) again remained unchanged.

LTβR–Ig induced lung regeneration was similar to that triggered by treatment with CHIR99021 alone (Fig. 4b). By contrast, lung regeneration was significantly reduced by PRI-724 (Fig. 4b). This was accompanied by a significant reduction in AXIN2-positive alveolar epithelial cells after treatment with cigarette smoke and Ig or cigarette smoke with LTβR–Ig and PRI-724 (Fig. 4c). Notably, exposure to cigarette smoke and LTβR–Ig or CHIR99021 restored the number of AXIN2-positive epithelial cells (Fig. 4c). These data were also corroborated by analysis of *Axin2* mRNA expression (Extended Data Fig. 10d). To test AT2 progenitor cell function, primary human AT2 cells were subjected to a lung organoid assay[35]. Organoid growth by human primary AT2 cells was functionally impaired by the activation of LTβR signalling (Fig. 4d, Extended Data Fig. 10e). However, this phenotype was partially restored by activating WNT/β-catenin signalling with CHIR99021 and LiCl (Fig. 4d, Extended Data Fig. 10f).

In summary, by analysis of lung tissue from patients with COPD and distinct mouse models, we identified increased *Lta* and *Ltb* expression by B and T cells, and *Tnfsf14* expression by T cells and granulocytes. We demonstrated a concept that therapeutic inhibition of LTβR signalling restores lung architecture from smoking induced-emphysema and airway fibrosis. Blocking LTβR signalling abolished the formation of

Article

iBALT, apoptosis of alveolar epithelial cells and re-initiated endogenous WNT/β-catenin-driven alveolar regeneration. Mechanistically, activation of LTβR signalling in progenitor AT2 cells decreased WNT/β-catenin activity via non-canonical NF-κB signalling, through the non-canonical NIK (Extended Data Fig. 10g).

In this study, analysis was of lungs solely derived from patients with end-stage COPD, this limited our ability to deduce the earliest time points of iBALT or LTβR-signalling during the progression of COPD immunopathogenesis. However, it has been shown recently that iBALT formation starts to become prevalent from moderate state of early COPD onwards, correlating with emphysema severity[10,12]. We believe it is imperative to conduct future (pre-)clinical studies that incorporate LTβR blockers and WNT/β-catenin activators as a potential dual therapeutic approach. Our reported findings in chronic smoking-induced lung tissue pathogenesis may have additional implications in the context of other diseases associated with tertiary lymphoid structures or LTβR signalling, airway fibrosis and tissue regeneration, beyond COPD.

Online content

Any methods, additional references, Nature Research reporting summaries, source data, extended data, supplementary information, acknowledgements, peer review information; details of author contributions and competing interests; and statements of data and code availability are available at https://doi.org/10.1038/s41586-020-2882-8.

1. Kratz, A., Campos-Neto, A., Hanson, M. S. & Ruddle, N. H. Chronic inflammation caused by lymphotoxin is lymphoid neogenesis. *J. Exp. Med.* **183**, 1461–1472 (1996).
2. Drayton, D. L., Liao, S., Mounzer, R. H. & Ruddle, N. H. Lymphoid organ development: from ontogeny to neogenesis. *Nat. Immunol.* **7**, 344–353 (2006).
3. Hogg, J. C. et al. The nature of small-airway obstruction in chronic obstructive pulmonary disease. *N. Engl. J. Med.* **350**, 2645–2653 (2004).
4. Galkina, E. & Ley, K. Immune and inflammatory mechanisms of atherosclerosis*. *Annu. Rev. Immunol.* **27**, 165–197 (2009).
5. Pitzalis, C., Jones, G. W., Bombardieri, M. & Jones, S. A. Ectopic lymphoid-like structures in infection, cancer and autoimmunity. *Nat. Rev. Immunol.* **14**, 447–462 (2014).
6. Senda, T. et al. Microanatomical dissection of human intestinal T-cell immunity reveals site-specific changes in gut-associated lymphoid tissues over life. *Mucosal Immunol.* **12**, 378–389 (2019).
7. Lozano, R. et al. Global and regional mortality from 235 causes of death for 20 age groups in 1990 and 2010: a systematic analysis for the Global Burden of Disease Study 2010. *Lancet* **380**, 2095–2128 (2012).
8. Vogelmeier, C. F. et al. Global Strategy for the Diagnosis, Management, and Prevention of Chronic Obstructive Lung Disease 2017 Report. GOLD Executive Summary. *Am. J. Respir. Crit. Care Med.* **195**, 557–582 (2017).
9. Baarsma, H. A. & Königshoff, M. 'WNT-er is coming': WNT signalling in chronic lung diseases. *Thorax* **72**, 746–759 (2017).
10. Polverino, F. et al. B cell-activating factor. An orchestrator of lymphoid follicles in severe chronic obstructive pulmonary disease. *Am. J. Respir. Crit. Care Med.* **192**, 695–705 (2015).
11. Faner, R. et al. Network analysis of lung transcriptomics reveals a distinct B-cell signature in emphysema. *Am. J. Respir. Crit. Care Med.* **193**, 1242–1253 (2016).
12. Sullivan, J. L. et al. B cell adaptive immune profile in emphysema-predominant COPD. *Am. J. Respir. Crit. Care Med.* **200**, 1434–1439 (2019).
13. Bracke, K. R. et al. Role of CXCL13 in cigarette smoke-induced lymphoid follicle formation and chronic obstructive pulmonary disease. *Am. J. Respir. Crit. Care Med.* **188**, 343–355 (2013).
14. Jia, J. et al. Cholesterol metabolism promotes B-cell positioning during immune pathogenesis of chronic obstructive pulmonary disease. *EMBO Mol. Med.* **10**, e8349 (2018).
15. Wolf, M. J., Seleznik, G. M., Zeller, N. & Heikenwalder, M. The unexpected role of lymphotoxin beta receptor signaling in carcinogenesis: from lymphoid tissue formation to liver and prostate cancer development. *Oncogene* **29**, 5006–5018 (2010).
16. Finkin, S. et al. Ectopic lymphoid structures function as microniches for tumor progenitor cells in hepatocellular carcinoma. *Nat. Immunol.* **16**, 1235–1244 (2015).
17. Xiao, G., Harhaj, E. W. & Sun, S. C. NF-κB-inducing kinase regulates the processing of NF-κB2 p100. *Mol. Cell* **7**, 401–409 (2001).
18. Dejardin, E. et al. The lymphotoxin-β receptor induces different patterns of gene expression via two NF-κB pathways. *Immunity* **17**, 525–535 (2002).
19. Fava, R. A. et al. A role for the lymphotoxin/LIGHT axis in the pathogenesis of murine collagen-induced arthritis. *J. Immunol.* **171**, 115–126 (2003).
20. Haybaeck, J. et al. A lymphotoxin-driven pathway to hepatocellular carcinoma. *Cancer Cell* **16**, 295–308 (2009).
21. Uhl, F. E. et al. Preclinical validation and imaging of Wnt-induced repair in human 3D lung tissue cultures. *Eur. Respir. J.* **46**, 1150–1166 (2015).
22. Alsafadi, H. N. et al. Applications and approaches for 3D precision-cut lung slices: disease modeling and drug discovery. *Am. J. Respir. Cell Mol. Biol.* **62**, 681–691 (2020).
23. Verhamme, F. M., Bracke, K. R., Joos, G. F. & Brusselle, G. G. Transforming growth factor-β superfamily in obstructive lung diseases. more suspects than TGF-β alone. *Am. J. Respir. Cell Mol. Biol.* **52**, 653–662 (2015).
24. Rabe, K. F. & Watz, H. Chronic obstructive pulmonary disease. *Lancet* **389**, 1931–1940 (2017).
25. Sandri, M. et al. PGC-1α protects skeletal muscle from atrophy by suppressing FoxO3 action and atrophy-specific gene transcription. *Proc. Natl Acad. Sci. USA* **103**, 16260–16265 (2006).
26. Lee, H. Y. et al. Targeted expression of catalase to mitochondria prevents age-associated reductions in mitochondrial function and insulin resistance. *Cell Metab.* **12**, 668–674 (2010).
27. John-Schuster, G. et al. Inflammaging increases susceptibility to cigarette smoke-induced COPD. *Oncotarget* **7**, 30068–30083 (2016).
28. Boutaffala, L. et al. NIK promotes tissue destruction independently of the alternative NF-κB pathway through TNFR1/RIP1-induced apoptosis. *Cell Death Differ.* **22**, 2020–2033 (2015).
29. Nabhan, A. N., Brownfield, D. G., Harbury, P. B., Krasnow, M. A. & Desai, T. J. Single-cell Wnt signaling niches maintain stemness of alveolar type 2 cells. *Science* **359**, 1118–1123 (2018).
30. Zacharias, W. J. et al. Regeneration of the lung alveolus by an evolutionarily conserved epithelial progenitor. *Nature* **555**, 251–255 (2018).
31. Kneidinger, N. et al. Activation of the WNT/β-catenin pathway attenuates experimental emphysema. *Am. J. Respir. Crit. Care Med.* **183**, 723–733 (2011).
32. de Leon-Boenig, G. et al. The crystal structure of the catalytic domain of the NF-κB inducing kinase reveals a narrow but flexible active site. *Structure* **20**, 1704–1714 (2012).
33. Tokunaga, Y. et al. Selective inhibitor of Wnt/β-catenin/CBP signaling ameliorates hepatitis C virus-induced liver fibrosis in mouse model. *Sci. Rep.* **7**, 325 (2017).
34. Ying, Q. L. et al. The ground state of embryonic stem cell self-renewal. *Nature* **453**, 519–523 (2008).
35. Hu, Y. et al. Wnt/β-catenin signaling is critical for regenerative potential of distal lung epithelial progenitor cells in homeostasis and emphysema. *Stem Cells* https://doi.org/10.1002/stem.3241 (2020).

[1]Comprehensive Pneumology Center (CPC), Institute of Lung Biology and Disease, Helmholtz Zentrum München, Member of the German Center for Lung Research (DZL), Neuherberg, Germany. [2]German Cancer Research Center (DKFZ), Division of Chronic Inflammation and Cancer, Heidelberg, Germany. [3]Comprehensive Pneumology Center (CPC), Lung Repair and Regeneration Research Unit, Helmholtz Zentrum München, Member of the German Center for Lung Research (DZL), Munich, Germany. [4]Division of Pulmonary Sciences and Critical Care Medicine, University of Colorado, Denver, CO, USA. [5]Laboratory of Molecular Immunology and Signal Transduction, GIGA-Institute, University of Liège, Liège, Belgium. [6]Institute of Computational Biology (ICB), Helmholtz Zentrum München, Neuherberg, Germany. [7]Department of Molecular Pharmacology, Groningen Research Institute for Asthma and COPD (GRIAC), University of Groningen, Groningen, The Netherlands. [8]Department of Hepatology & Gastroenterology, Charité University Medicine Berlin, Berlin, Germany. [9]German Cancer Research Center (DKFZ), Division of Signaling and Functional Genomics, Heidelberg, Germany. [10]Division of Pneumology, KU Leuven, Leuven, Belgium. [11]Lung Bioengineering and Regeneration, Department of Experimental Medical Sciences, Lund University, Lund, Sweden. [12]Asklepios Fachkliniken Munich-Gauting, Member of the German Center for Lung Research (DZL), Munich, Germany. [13]Translational Lung Research and CPC-M bioArchive, Comprehensive Pneumology Center, Helmholtz Zentrum München, Member of the German Center for Lung Research (DZL), Munich, Germany. [14]Institute of Experimental Genetics, German Mouse Clinic, Helmholtz Zentrum München, Neuherberg, Germany. [15]Institute of Molecular Immunology & Experimental Oncology, Klinikum rechts der Isar, Technical University of Munich, Munich, Germany. [16]Emmy Noether Research Group Epigenetic Machineries and Cancer, Division of Chronic Inflammation and Cancer, German Cancer Research Center (DKFZ), Heidelberg, Germany. [17]Laboratory of Medicinal Chemistry, Center for Interdisciplinary Research on Medicines (CIRM), University of Liège, Liège, Belgium. [18]Experimental Genetics, Technische Universität München, Freising, Germany. [19]German Center for Diabetes Research (DZD), Neuherberg, Germany. [20]Medical Faculty Mannheim & BioQuant, Heidelberg University, Heidelberg, Germany. [21]These authors contributed equally: Thomas M. Conlon, Gerrit John-Schuster, Mathias Heikenwalder, Ali Önder Yildirim. ✉e-mail: m.heikenwaelder@dkfz.de; oender.yildirim@helmholtz-muenchen.de

Methods

Human lung tissue core sampling

Lung core samples from explanted lungs of patients with COPD undergoing lung transplantation were provided by S. Verleden (University of Leuven, Belgium) following ethical approval of the University of Leuven Institutional Review Board (ML6385). Patient demographics are highlighted in Supplementary Table 1. Immediately after transplant, lungs were air-inflated at 10 cm H_2O pressure and fixed using constant pressure in the fumes of liquid nitrogen. Afterwards lungs were sliced using a band saw and sampled using a core bore. All participants provided informed written consent. For controls, unused donor lungs were collected under existing Belgian law which allows the use of declined donor lungs for research after second opinion inspection, and processed as above. Lungs were declined for various reasons (kidney tumour, logistics, presence of microthrombi). Upon receipt, lung cores were portioned for fixation in 4% paraformaldehyde followed by paraffin embedding, and total RNA isolation (peqGOLD Total RNA Kit, Peqlab).

Human precision cut lung slices

Tumour-free tissue from six patients who underwent lung tumour resection was used for the preparation of precision-cut lung slices (PCLS) as previously described[21]. Tissue was provided by the Asklepios Biobank for Lung Diseases (Gauting, Germany; project number 333-10). All participants provided informed written consent, and the use of human tissue approved by the ethics committee of the Ludwig-Maximillian University (Munich, Germany; project number 455-12). PCLS were cultivated in DMEM/Ham's F12 medium supplemented with 0.1% FBS (Gibco, Life Technologies), 100 U ml^{-1} penicillin-streptomycin and 2.5 µg ml^{-1} amphotericin B (Sigma) at 37 °C in 5% CO_2 atmosphere, and stimulated for 24 h with 10 µg ml^{-1} LPS (*E. coli* O55:B5, Sigma-Aldrich), 1 µg ml^{-1} human LTβR–Ig fusion protein (supplied by J. Browing, Biogen Idec), 20 ng ml^{-1} recombinant human TNF (300-01A, PeproTech) or 2 µg ml^{-1} agonistic antibody to human LTβR (clone BS1, Biogen Idec). Total RNA was isolated using peqGOLD Total RNA Kit (Peqlab).

Human lung organoid culture

Fresh human lung tissue from de-identified healthy donors were obtained through National Jewish hospital Human Lung Tissue Consortium (HLTC) and used following ethical approval by the Institutional Review Board of the University of Colorado and National Jewish Hospital under IRB exempt HS-2598. The HLTC obtains fresh lungs from Donor Alliance, our local organ procurement agency and the International Institute for the Advancement of Medicine. Primary human ATII cells were isolated as described previously[36]. Human lung organoid culture was adapted from previously described mouse lung organoid culture system[37,38]. In brief, MRC-5 human fetal lung fibroblasts (ATCC) were proliferation-inactivated with 10 µg ml^{-1} mitomycin C (Sigma Aldrich) for 2 h. Approximately 10,000 primary human lung EpCAM-positive cells were resuspended in 50 µl medium and diluted 1:1 with 10,000 MRC-5 cells in 50 µl growth factor-reduced Matrigel (Corning). Cell mixture was seeded into 24-well plate 0.4-µm transwell inserts (Corning). Cultures were treated from day 0 and every second or third day in DMEM/F12 containing 5% FBS, 100 U ml^{-1} penicillin/streptomycin, 2 mM L-alanyl-L-glutamine, amphotericin B (Gibco), insulin-transferrin-selenium (Gibco), 0.025 µg ml^{-1} recombinant human EGF (Sigma Aldrich), 0.1 µg ml^{-1} Cholera toxin (Sigma Aldrich), 30 µg ml^{-1} bovine pituitary extract (Sigma Aldrich), and 0.01 µM freshly added all-trans retinoic acid (Sigma Aldrich). Y-27632 (Tocris) (10 µM) was added for the first 48 h of culture. Organoids were imaged at day 14 using a Cytation1 cell imaging reader running Gen5 v3.08 software (Biotek) and quantified through ImageJ software (v1.52a).

Animals and maintenance

Eight-to-ten-week-old and 12-month-old pathogen-free female C57BL/6 mice were obtained from Charles River and housed in rooms maintained at a constant temperature of 20–24 °C and 45–65% humidity with a 12 h light cycle. Mice were allowed food and water ad libitum. Mice were randomly allocated into experimental groups with no statistical methods used to predetermine sample size. Sample sizes were chosen based on similar studies from the literature by ourselves and others and sufficient to detect statistically significant differences between groups. Quantitative morphometry on lung sections from mice was undertaken by readers blinded to the study groups. All animal experiments were approved by the ethics committee for animal welfare of the local government for the administrative region of Upper Bavaria (Regierungspräsidium Oberbayern) and were conducted under strict governmental and international guidelines in accordance with EU Directive 2010/63/EU.

Cigarette smoke exposure and LTβR–Ig treatment

Cigarette smoke was generated from 3R4F Research Cigarettes (Tobacco Research Institute, University of Kentucky), with the filters removed. Mice were whole-body-exposed to active 100% mainstream cigarette smoke of 500 mg m^{-3} total particulate matter (TPM) for 50 min twice per day for 4 and 6 months in a manner mimicking natural human smoking habits as previously described[39]. The TPM level was monitored via gravimetric analysis of quartz fibre filters before and after sampling air from the exposure chamber and measuring the total air volume. CO concentrations in the exposure chamber were constantly monitored by using a GCO 100 CO Meter (Greisinger Electronic) and reached values of 288 ± 74 ppm. All mice tolerated CS-mediated CO concentrations without any sign of toxicity, with CO-Hb levels of 12.2 ± 2.4%.

In two parallel experiments, mice were treated with an LTβR–Ig fusion protein[19] (80 µg intraperitoneally, weekly) (muLTβR-muIgG, supplied by J. Browing, Biogen Idec) or control-Ig (MOPC21, Biogen Idec) for 2 months, starting from 2 and 4 months of cigarette smoke exposure. Control mice were kept in a filtered air environment, but exposed to the same stress as cigarette smoke-exposed animals. Twenty-four hours after the last exposure to cigarette smoke, mice were killed. Experiments were performed twice, with $n = 8$ animals per group.

Elastase application and LTβR–Ig treatment

Emphysema was induced in mice by a single oropharyngeal application of PPE (40 U kg^{-1} body weight in 80 µl volume) as previously described[40]. Control mice received 80 µl of sterile PBS. Starting from day 28 after elastase application, mice were treated with an LTβR–Ig fusion protein (80 µg i.p., weekly) or control-Ig for 2 months. Experiments were performed twice, with $n = 8$ mice per group.

Four-paw muscle strength test

A grip strength meter system (Bioseb) was used to assess muscle strength in the mice. Mice holding onto a grid with four paws are slowly pulled away, the maximum force is recorded when the mouse releases the grid[41]. Each mouse was assessed three times over 1 min, with the mean value being taken to represent the strength of an individual mouse. Body weight was also measured and taken into account for analysis.

Lung function measurements

Mice were anaesthetized with ketamine-xylazine, tracheostomized and the diffusing capacity for carbon monoxide (DFCO) calculated[42]. In brief, 0.8 ml mixed gas (0.5% Ne, 21% O_2, 0.5% CO and 78% N_2) was instilled into the mice lungs and withdrawn 2 s later for analysis on a 3000 Micro GC Gas Analyzer (Infinicon) running EZ IQ software v.3.3.2 (Infinicon). DFCO was calculated as $1 - (CO_1/CO_0)/(Ne_1/Ne_0)$, in which 0 and 1 refer to the gas concentration before and after instillation, respectively. Respiratory function was measured using a flexiVent system running Flexiware v.7.6.4 software (Scireq). Mice were ventilated with a tidal volume of 10 ml kg^{-1} at a frequency of 150 breaths per min to reach a mean lung volume similar to that of spontaneous

breathing. Testing of lung mechanical properties including dynamic lung compliance was carried out by a software-generated script that took four readings per mouse.

Lung tissue processing

The right lung lobes were snap frozen in liquid nitrogen, homogenized and total RNA isolated (peqGOLD Total RNA Kit, Peqlab). The left lobe was fixed at a constant pressure (20 cm fluid column) by intratracheal instillation of PBS buffered 6% paraformaldehyde and embedded into paraffin for histological analysis of haematoxylin and eosin (H&E) or Masson's Trichrome stained sections and for immunohistochemistry.

Generation of single-cell suspensions from whole mouse lung tissue

Lung single-cell suspensions were generated as previously described[43,44]. In brief, after euthanasia, lung tissue was perfused with sterile saline through the heart and the right lung was tied off at the main bronchus. The left lung lobe was subsequently filled with 4% paraformaldehyde for later histologic analysis. Right lung lobes were removed, minced (tissue pieces at approximately 1 mm^2), and transferred for mild enzymatic digestion for 20–30 min at 37 °C in an enzymatic mix containing dispase (50 caseinolytic U ml^{-1}), collagenase (2 mg ml^{-1}), elastase (1 mg ml^{-1}), and DNase (30 µg ml^{-1}). Single cells were collected by straining the digested tissue suspension through a 40-µm mesh. After centrifugation at 300g for 5 min, single cells were taken up in 1 ml of PBS (supplemented with 10% fetal calf serum), counted and critically assessed for single cell separation and overall cell viability. For Dropseq, cells were aliquoted in PBS supplemented with 0.04% of bovine serum albumin at a final concentration of 100 cells µl^{-1}.

scRNA-seq using Dropseq

Dropseq experiments were performed according to previously published protocols[43,45]. Using a microfluidic device, single cells (100 per µl) were co-encapsulated in droplets with barcoded beads (120 per µl; purchased from ChemGenes Corporation) at rates of 4,000 µl h^{-1}. Droplet emulsions were collected for 10–20 min each before droplet breakage by perfluorooctanol (Sigma-Aldrich). After breakage, beads were harvested and the hybridized mRNA transcripts reverse transcribed (Maxima RT, Thermo Fisher). Unused primers were removed by the addition of exonuclease I (New England Biolabs). To improve the quality of the single cell transcripts and later the sequencing recovery, beads were subjected to Klenow enzyme treatment, as described for the Seq-Well single cell protocol[46]. In brief, beads were incubated in freshly prepared 0.1 M NaOH for 5 min while rotating and washed using TE-buffer (10mM Tris at pH 8.0, 1mM EDTA), supplemented with 0.01% Tween-20 (TE-TW buffer). Subsequently, beads were washed in TE-TW buffer and 1× TE buffer. Beads were resuspended in 200 µl per sample Klenow mix (see Seq-well protocol for details[46]) and incubated for 1 h at 37 °C at end-over-end rotation. After Klenow enzymatic treatment, beads were washed, counted, and aliquoted for pre-amplification (2,000 beads per reaction, equals approximately 100 cells per reaction) with 12 PCR cycles (Smart PCR primer: AAGCAGTGGTATCAACGCAGAGT (100 µM), 2x KAPA HiFi Hotstart Ready-mix (KAPA Biosystems), cycle conditions: 3 min 95 °C, 4 cycles of 20 s 98 °C, 45 s 65 °C, 3 min 72 °C, followed by 9 cycles of 20 s 98 °C, 20 s 67 °C, 3 min 72 °C, then 5 min at 72 °C). PCR products of each sample were pooled and purified twice by 0.6x clean-up beads (CleanNA), following the manufacturer's instructions. Before tagmentation, complementary DNA (cDNA) samples were loaded on a DNA High Sensitivity Chip on the 2100 Bioanalyzer (Agilent) to ensure transcript integrity, purity, and amount. For each sample, 1 ng of pre-amplified cDNA from an estimated 1500 cells was tagmented by Nextera XT (Illumina) with a custom P5-primer (Integrated DNA Technologies). Single-cell libraries were sequenced in a 100 bp paired-end run on the Illumina HiSeq4000 using 0.2 nM denatured sample and 5% PhiX spike-in. For priming of read 1, 0.5 µM Read1CustSeqB (primer

sequence: GCCTGTCCGCGGAAGCAGTGGTATCAACGCAGAGTAC) was used.

scRNA-seq data analysis

After sequencing, the processing of next-generation sequencing reads of the scRNA-seq data was performed as previously described[45]. In brief, the Drop-seq computational pipeline was used (v.2.3.0) as previously described and STAR (v.2.5.3a) was used for the alignment of reads to the mm10 reference genome (provided by the Drop-seq group, GSE63269). For barcode filtering, we excluded barcodes with less than 200 detected genes.

Downstream analysis was performed using the Scanpy package[47]. During preprocessing steps, we assessed the quality of our libraries and applied suitable filter criteria motivated by previously described best practices[48] with slight adjustments. After exploration of UMI counts and genes per cell for the combined count matrices, we retained barcodes with count numbers in the range of 400 to 6,000 counts per cell and genes detected in at least 3 cells. A high proportion of transcript counts derived from mitochondria-encoded genes may indicate low cell quality, and we removed cells with a percentage of mitochondrial transcripts of larger than 20%.

The expression matrices were normalized with scran's size factor based approach[49] and log transformed via scanpy's pp.log1p() function. In an additional step to mitigate the effects of unwanted sources of cell-to-cell variation, we calculated and regressed out the cell cycle score for each cell. Variable genes were selected sample-wise, excluding known cell cycle genes. Those genes being ranked among the top 4,000 in at least 3 samples were used as input for principal component analysis. Clustering was performed via scanpy's louvain method at resolution 2 and cell types manually annotated by using known marker genes. We encountered one unidentifiable cluster marked by low number of counts and high proportion of mitochondrial transcript-enriched cells, thus we marked these cells as unqualified and additionally filtered it out. The visualization was obtained with the UMAP embedding specifying the input parameters as 50 principal components and 20 nearest neighbours. The final object encompassed 25,095 genes across 21,413 cells.

Scoring for enrichment of gene signatures of interest was performed by using scanpy's tl.score_genes() function and the following gene lists: (1) apoptosis score: 157 genes from our dataset overlapping with Hallmark Apoptosis list from MSigDB; (2) positive regulation of NIK/NF-κB signalling: 76 genes associated with the corresponding Gene Ontology (GO) term GO:1901224. Statistical significance was assessed by using Wilcoxon rank-sum test on normalized, log-transformed count values and corrected with Benjamini–Hochberg. scRNA-seq metadata can be found in Supplementary Table 4. All code used for data visualization of the scRNA-seq data can be found at https://github.com/theislab/2020_Inhibition_LTbetaR-signalling.

Proteome analysis of whole lung homogenates

Proteins have been loaded on SDS–PAGE gel, which ran only a short distance of 0.5 cm. After Commassie staining the total sample was cut out unfractionated and used for subsequent trypsin digestion according to a slightly modified previously described protocol[50] carried out on the DigestPro MSi robotic system (INTAVIS Bioanalytical Instruments AG).

Digested samples have been loaded on a cartridge trap column, packed with Acclaim PepMap300 C18, 5 µm, 300 Å wide pore (Thermo Fisher Scientific) and separated in a 180 min gradient from 3% to 40% ACN on a nanoEase MZ Peptide analytical column (300 Å, 1.7 µm, 75 µm × 200 mm, Waters) and a UltiMate 3000 UHPLC system. Furthermore, eluting peptides have been analysed by an online coupled Q-Exactive-HF-X mass spectrometer running software version Exactive Series 2.9 (Thermo Fisher Scientific) in a data depend acquisition mode where one full scan was followed by up to 12 MS–MS scans of eluting peptides.

Proteomic data analysis

Mass spectrometry raw files were processed using the MaxQuant software[51] (v.1.6.12.0). As previously described[52], peak lists were searched against the mouse Uniprot FASTA database (version November 2016), and a common contaminants database by the Andromeda search engine.

All statistical and bioinformatics operations such as normalization, principal component analysis, annotation enrichment analysis and hierarchical clustering of z-scored MS-intensities were run with the Perseus software package (v.1.6.10.50)[53]. Proteomics data can be found in Supplementary Table 5.

Microarray analysis

Total RNA was isolated using the RNeasy Mini Kit (Qiagen) from the lungs of C57BL/6 mice exposed to filtered air for 6 months ($n = 3$), cigarette smoke for 6 months ($n = 3$) and cigarette smoke for 6 months plus the LTβR–Ig fusion protein for the last 2 months (therapeutic protocol, $n = 3$) as described above. RNA quality was assessed using an Agilent 2100 Bioanalyzer, with high-quality RNA (RNA integrity number (RIN) > 7) being used for analysis. Three-hundred nanograms of total RNA was amplified using the Illumina TotalPrep RNA Amplification kit (Ambion), then hybridized to Mouse Ref-8 v2.0 Expression BeadChips (Illumina). Staining and scanning were undertaken according to the Illumina expression protocol. Data were processed using the GenomeStudioV2010.1 software (gene expression module v.1.6.0) in combination with the MouseRef-8_V2_0_R3_11278551_A.bgx annotation file. The background subtraction option was used and an offset to remove remaining negative expression values introduced. CARMAweb was used for quantile normalization[54]. Statistical analyses were performed by using the statistical programming environment R (v.3.2.3, R Development Core Team), implemented in CARMAweb. Genewise testing for differential expression was carried out using the limma t-test and Benjamini–Hochberg multiple testing correction (false discovery rate (FDR) < 10%). Heat maps were generated using Genesis software (release 1.7.7, Institute for Genomics and Bioinformatics, Graz University of Technology).

Flow cytometry analysis of lung

Single-cell suspension was derived by using MACS Dissociator (Miltenyi Biotech) according to manufacturer's instructions. Staining was performed using Live/Dead discrimination by ZombieDyeNIR according to the manufacturer's instructions for lymphocytes and Live/Dead discrimination by fixable viability stain FVS620 (BD) for myeloid cells. After washing (approximately $400g$, 5 min, 4 °C), cells were stained in 25 µl of titrated antibody master mix for 20 min protected from light at 4 °C and washed again[55]. Cells were analysed using BD FACSFortessa running FACSDiva software v8.0.1. Data were analysed using Flowlogic v7.3 and FlowJo v10.6.1. For t-SNE representation, myeloid cells were downsampled to 3,000 live CD45$^+$CD11b$^+$ and/or CD11c$^+$ cells; and lymphocytes were downsampled to 5,000 live CD45$^+$ cells. Antibodies used are shown in Supplementary Table 2.

qRT–PCR

cDNA was synthesized from 1 µg total RNA using Random Hexamers and MuLV Reverse Transcriptase (Applied Biosystems). mRNA expression was analysed using Platinum SYBR Green qPCR SuperMix (Applied Biosystems) on a StepOnePlus 96 well Real-Time PCR System (Applied Biosystems). Primers were designed using Primer-BLAST software (https://www.ncbi.nlm.nih.gov/tools/primer-blast/) or obtained from PrimerBank[56] (https://pga.mgh.harvard.edu/primerbank/). Primer sequences are listed in Supplementary Table 3. Relative expression of each gene was calculated relative to the housekeeping gene *HPRT1* or *Hprt1* as $2^{-\Delta Ct}$, and fold changes compared to control samples as $2^{-\Delta\Delta Ct}$ values. Relative changes of selected genes were also presented as a heat map generated by Genesis software (Release 1.7.7, Institute for Genomics and Bioinformatics, Graz University of Technology).

Immunohistochemistry

Three-micrometres sections from human core samples or mouse left lung were deparaffinizing in xylene and rehydrated before treatment with 1.8% (v/v) H$_2$O$_2$ solution (Sigma-Aldrich) to block endogenous peroxidase. Heat-induced epitope retrieval was performed in HIER citrate buffer (pH 6.0, Zytomed Systems) in a decloaking chamber (Biocare Medical). To inhibit nonspecific binding of antibodies, sections were treated with a blocking antibody (Biocare Medical). After overnight incubation with primary antibodies at 4 °C sections were incubated with an alkaline phosphatase or horseradish peroxidase (HRP)-conjugated secondary antibody (Biocare Medical). Signals were amplified by adding chromogen substrate Vulcan fast red or 3,3′-diaminobenzidine (DAB) (Biocare Medical), respectively. Sections were counterstained with haematoxylin (Sigma-Aldrich) and dehydrated in xylene and mounted. Primary antibodies: rabbit anti-RelA/p65 (1:500, clone A, sc-109, Santa Cruz), rabbit anti-RELB (1:400, clone C-19, sc-226, Santa Cruz), mouse anti-CD20 (1:100, clone L26, MSK008, Zytomed Systems), rat anti-B220 (1:3,000, clone RA3-6B2, 553084, BD Biosciences), rabbit anti-CD3 (1:500, clone SP7, RBK024, Zytomed Systems), rabbit anti-CD68 (1:100, polyclonal, ab125212, Abcam), rabbit anti-Collagen I (1:250, polyclonal, ab21286, Abcam), rabbit anti-pSMAD2 (1:500, polyclonal, AB3849, Merck Millipore), mouse anti-hLTB (1:1,000, clone B27, supplied by J. Browing, Biogen Idec), rabbit anti-cleaved caspase3 (1:300, polyclonal, 9661, Cell Signaling Technology), rabbit anti-TCF4 (1:100, polyclonal, ab185736, Abcam) and rabbit anti-AXIN2 (1:2,000, polyclonal, ab32197, Abcam).

Multiplex immunofluorescence staining

Sequential immunostaining was performed on 3-µm thick formalin-fixed paraffin-embedded mouse lung sections. In brief, heat-mediated antigen retrieval was performed in citrate pH 6.0 (antibody Mix 1, ThermoFisher), or in EDTA pH 9.0 (antibody mix 2, Novus) buffer. Antibody elution was performed between each staining cycle[57]. Antibodies used in mix 1 were: rat anti-CD4 (1:200, ThermoFisher 14-9766-82), rat anti-CD8a (1:200, ThermoFisher 14-0808-82) and rat anti-B220 (1:500, Biolegend 103202). Antibodies used in mix 2 were: rabbit anti-IBA1 (1:1.000, VWR 100369-764), rabbit anti-iNOS (1:100, Abcam ab15323) and rabbit anti-CD206 (1:500, ProteinTech 18704-1-AP). Secondary antibodies used were: anti-rabbit 555 (1:500, Cell Signaling 4413S), anti-rabbit 647 (1:500, Cell Signaling 4414S) and anti-rat 647 (1:500, Cell Signaling 4418S).

Acquired images were processed using FIJI and the FIJI plugin HyperStackReg V5.6[58] (and Ved Sharma 13 December 2018). ImageJ plugin HyperStackReg V5.6 (Zenodo. https://doi.org/10.5281/zenodo.2252521). Autofluorescence acquired in non-relevant channels was substracted as appropriate. IBA1 and iNOS staining quantitation was performed using Ilastik (v.1.3.3post2)[59] and CellProfiler (v.3.1.9)[60].

RNA in situ hybridization

Five-micrometre sections from paraffin-embedded mouse left lung or human core samples were used for in situ hybridization using the RNAscope 2.5 HD Assay- BROWN (Advanced Cell Diagnostics) according to manufacturer's instructions and the RNAscope EZ-Batch Slide Processing System (Advanced Cell Diagnostics). The following probes from Advanced Cell Diagnostics were used; RNAscope Probe-Mm-Lta (317231), RNAscope Probe-Mm-Ltb (315681), RNAscope Probe-Mm-Tnfsf14 (411111), RNAscope Probe-Mm-TNFa (311081), RNAscope Probe-Hs-LTA (310461) and RNAscope Negative Control Probe – DapB (310043).

Quantitative morphometry

Design-based stereology was used to analyse sections using an Olympus BX51 light microscope equipped with a computer-assisted stereological

toolbox (newCAST, Visiopharm) running Visiopharm Integrator System (VIS) v.6.0.0.1765 software, on H&E or Masson's Trichrome stained lung tissue sections as previously described[61,62]. Air space enlargement was assessed by quantifying mean linear chord length (MLI) and alveolar surface density on 30 fields of view per lung using the ×20 objective. In brief, a line grid was superimposed on lung section images. Intercepts of lines with alveolar septa and points hitting air space were counted to calculate MLI applying the formula $MLI = \sum P_{air} \times L(p) / \sum I_{septa} \times 0.5$. P_{air} are the points of the grid hitting air spaces, $L(p)$ is the line length per point, I_{septa} is the sum of intercepts of alveolar septa with grid lines. Alveolar surface density was calculated applying the formula: surface density $= 2 \times \sum I_{septa} / \sum P_{septa} \times L(p)$, where P_{septa} are the points of the grid hitting alveolar septa.

Volume of iBALT and airway collagen normalized to the basal membrane was quantified on 50 fields of view per lung (using the ×40 objective) by counting points hitting iBALT (P_{iBALT}) or airway collagen ($P_{collagen}$) and intercepts of lines with airways and vessels ($I_{airway + vessel}$). The volume was calculated by applying the formula $V/S = \sum P_{iBALT/collagen} \times L(p) / \sum I_{airway + vessel}$. Furthermore, the total number of iBALT was quantified in a whole lung tissue slide and normalized to total number of airways.

For quantification of immunohistochemistry stained lung tissue sections 20 random fields of view were assessed across each lung using the CAST system and ×40 objective. The total number of CD68-positive cells was recorded. For RELA, RELB, caspase-3, AXIN2 and TCF4 counting the number of positive alveolar epithelial cells out of the total number of alveolar epithelial cells were recorded as a percentage.

Western blotting

Twenty micrograms of protein was separated by SDS−PAGE, transferred onto a polyvinylidene difluoride membrane (Bio-Rad), blocked with 5% non-fat milk and immunoblotted overnight at 4 °C with antibodies against RELB (1:1,000, clone D7D7W, 10544, Cell Signaling), p52 (and p100) (1:1,000, polyclonal, 4882, Cell Signaling), cleaved caspase-3 (1:1,000, polyclonal, Cell Signaling) and β-catenin (1:1,000, clone 14, 610154, BD Biosciences). Antibody binding was detected with HRP-conjugated secondary antibodies and developed using Amersham ECL Prime reagent (GE Healthcare). Bands were detected and quantified using the Chemidoc XRS+ system running ImageLab v.5.2.1 software (Bio-Rad) or using photographic film and ImageJ (v.1.49o), and normalized to β-actin levels (anti-β-actin-peroxidase conjugated mouse monoclonal antibody, 1:50,000, clone AC-15, A3854, Sigma-Aldrich), vinculin (anti-vinculin, 1:1,000, clone 7F9, sc-73614, Santa Cruz) or tubulin (anti-tubulin, 1:5,000, clone B-5-1-2, T6074, Sigma-Aldrich).

ELISA

Concentrations of active TGFβ in BAL fluid were determined using a commercially available kit for enzyme-linked immunosorbent assay (eBioscience, ThermoFisher Scientific).

Primary mouse AT2 cell isolation and culture

Primary mouse AT2 cells were isolated as previously described[63–66]. In brief, mouse lungs were intratracheally inflated with dispase (BD Bioscience) followed by 300 μl instillation of 1% low gelling temperature agarose (Sigma Aldrich,). Lungs were minced and filtered through 100-μm, 20-μm and 10-μm nylon meshes (Sefar). Negative selection of fibroblasts was performed by adherence on cell culture dishes for 30 min. Non-adherent cells were collected and white blood cells and endothelial cells were depleted with CD45 and CD31 magnetic beads respectively (Miltenyi Biotec), according to manufacturer's instructions. pmATII cells were resuspended in DMEM containing 10% FBS (Pan-Biotech), 2 mM L-glutamine (Life Technologies), 100 mg l⁻¹ streptomycin, and 100 U ml⁻¹ penicillin (Sigma Aldrich), 3.6 mg ml⁻¹ glucose (Applichem) and 10 mM HEPES (Life Technologies) and cultured for 48 h to allow attachment. Cells were starved with medium containing

0.1% FBS and finally treated for 24 h with an agonistic antibody to LTβR (2 μg ml⁻¹) (clone ACH6, supplied by J. Browing, Biogen Idec) and recombinant mouse WNT3A (100 ng ml⁻¹) (1324-WN, R&D Systems).

LA4 cell culture

The mouse AT2-like cell line LA4 (CCL-196, ATCC) was maintained in Ham's F12 medium containing NaHCO₃ and stable glutamine (Biochrom AG), supplemented with 15% fetal calf serum (Gibco, Life Technologies), 100 U ml⁻¹ penicillin-streptomycin (Sigma-Aldrich) and 1% non-essential amino acids (Biochrom AG) at 37 °C in 5% CO₂ atmosphere. The cell line was not authenticated. LA4 cell lines were routinely tested for mycoplasma, and tested negative.

For LA4 apoptosis measurements, cells were seeded at 1×10^5 cells per well in 24-well plates. Then, 24 h later, cells were stimulated for 6 and 24 h with an agonistic antibody to LTβR (2 μg ml⁻¹) (5G11, HM1079, Hycult Biotech), recombinant murine TNF (1 ng ml⁻¹) (315-01A, PeproTech) or a combination thereof. To inhibit apoptotic signalling, cells were co-stimulated with necrostatin-1 (50 μM) (N9037, Sigma-Aldrich) or Z-Val-Ala-DL-Asp-fluoromethylketone (z-VAD-FMK) (20 μM) (627610, Merck Millipore). Apoptosis levels were analysed using the Annexin V Apoptosis Detection Kit APC (eBioscience, ThermoFisher Scientific) and then stained cells were quantified on a BD FACSCanto II flow cytometer (BD Biosciences) with BD FACSDiva v.6.1.3 software.

For the LA4 wound-healing assay, a scratch was induced 24 h after seeding (time point 0 h) and cells were stimulated for 24 h as described above. Afterwards, cells were washed and cultured for a further 32 h (time point 56 h) in fresh medium. Wound closure was determined as the percentage of wound closure at 0 and 56 h using AxioVision software (v.4.9.1.0, Zeiss) to calculate the wound surface area.

To examine WNT signalling cells were seeded at 1×10^5 cells per well in 24-well plates. Then, 24 h later, cells were stimulated for 24 h with an agonistic antibody to LTβR (2 μg ml⁻¹) (clone ACH6, supplied by J. Browing, Biogen Idec), recombinant mouse TNF (1 ng ml⁻¹) (315-01A, PeproTech) or a combination thereof. In addition, cells were pre-treated for 1 h and then incubated for 24 h with necrostatin-1 (50 μM) (N9037, Sigma-Aldrich), TPCA-1 (10 μM) (T1452, Sigma-Aldrich) or BAY 11-7082 (10 μM) (B5556, Sigma-Aldrich). Total RNA was isolated using the peq-GOLD Total RNA Kit (Peqlab).

A549 and MLE12 cell culture

Both the human AT2-like cell line A549 (CCL-185, ATCC) and mouse AT2-like cell line MLE12 (CCL-2110, ATCC) were maintained in DMEM/F12 medium containing NaHCO₃ and stable glutamine (Biochrom AG), supplemented with 10% fetal calf serum (Gibco, Life Technologies) and 100 U ml⁻¹ penicillin-streptomycin (Sigma-Aldrich) at 37 °C in 5% CO₂ atmosphere. Both cell lines were not authenticated. Both cell lines were routinely tested for Mycoplasma, and tested negative.

For mRNA experiments cells were seeded in 24-well plates at 5×10^4 cells per well and for protein cells were seeded in 6-well plates at 2×10^5 cells per well. Twenty-four hours later, cells were stimulated in medium containing 0.1% fetal calf serum with, recombinant murine WNT3A (100 ng ml⁻¹, 1324-WN, R&D Systems or 315-20, Peprotech), CHIR99021 (1 μM, 4423, Tocris), an agonistic antibody to LTβR (for mouse 2 μg ml⁻¹ clone ACH6, for human 0.5 μg ml⁻¹ clone BS1 both supplied by J. Browing, Biogen Idec), recombinant mouse TNFSF14 (250–500 ng ml⁻¹, 664-LI-025/CF, R&D Systems), TPCA-1 (5 μM, T1452, Sigma-Aldrich) and bortezomib (10 nM, Millennium, Takeda). Total RNA was isolated using the peqGOLD Total RNA Kit (Peqlab) and cellular lysates prepared in RIPA buffer.

In additional experiments, MLE12 cells were pre-treated 2 h with the NIK kinase inhibitor (CMP1, 1 μM, prepared in house) and stimulated for 30 h with recombinant mouse WNT3A (200 ng ml⁻¹, 1324-WN, R&D Systems), an agonistic antibody to LTβR (2 μg ml⁻¹, clone ACH6) or recombinant Flag-TNFSF14 (200 ng ml⁻¹, ALX-522-018-C010, Alexis

Biochemicals). Cellular lysates were prepared in RIPA buffer for western blot analysis.

Synthesis of the NIK kinase inhibitor

The NIK kinase inhibitor (4-(1-(2-amino-5-chloro-4-pyrimidinyl)-2,3-dihydro-1H-indol-6-yl)-2-(1,3-thiazol-2-yl)-3-butyn-2-ol) CMP1, was obtained according to the synthetic process described in WO 2009/158011 A1. For the chemical structure, see Supplementary Fig. 1.

However, to improve the yields, the last step consisting of the Sonogashira coupling reaction between the aryl bromide and the alcyne using cuprous iodide and triethylamine as the catalysts in DMF was replaced by the use of palladium acetate and triphenylphosphine in the presence of DBU as the catalytic system in THF according to a recent publication[67].

WNT/β-catenin luciferase reporter assay

WNT/β-catenin signalling was measured as previously described[36]. In short, M50 Super 8x TOPflash and M51 Super 8x FOPflash plasmids[68], containing a firefly luciferase gene under the control of TCF/LEF binding sites (TOPflash) or mutated TCF/LEF binding sites (FOPflash) were used. MLE12 cells were plated in 48-well plates at a density of 55,000 cells per well. The next day cells were transfected with either 75 ng per well of M50 Super 8x TOPflash plasmid or the negative control M51 Super 8x FOPflash using Lipofectamine 2000 reagent (Life Technologies) in serum-free Opti-MEM medium (Life Technologies). After 6 h of transfection, cells were stimulated for 24 h with an agonistic antibody to LTβR (2 µg ml^{-1}) (clone ACH6, supplied by J. Browing, Biogen Idec), recombinant mouse TNF (1 ng ml^{-1}) (315-01A, PeproTech) and CHIR99021 (1 µM) (4423, Tocris). Cells were lysed using Glo lysis buffer and luciferase activity was assayed using the Bright-Glo luciferase assay system (Promega). Luciferase activity was determined using a luminescence plate reader (Berthold Technologies). Measured values were analysed with WinGlow Software (MikroWin v.4.41, Berthold Technologies) and TOPflash activity was normalized to FOPflash activity and expressed relative to control conditions.

GSEA

GSEA software (v.4.0.1) from the Broad Institute (http://www.gsea-msigdb.org/gsea/index.jsp)[69,70] was used to determine the enrichment of gene lists in our microarray data generated above, proteomic data generated above and data obtained from series matrix files downloaded from the NCBI GEO database (GSE47460–GPL14550[71], GSE37768, GSE56768 and GSE52509[61]). The following gene lists were examined; Hallmark collection v6.2 (Broad Institute), GO:0033209 tumour necrosis factor-mediated signalling pathway, GO:0051092 positive regulation of NF-κB transcription factor activity, GO:0043123 positive regulation of I-κB kinase NF-κB signalling, GO:0038061 NIK NF-κB signalling, GO:0008013 beta catenin binding, and GO:0060070 canonical WNT signalling. Gene lists for apoptosis were obtained from the Hallmark collection, and for LTβR signalling and NF-κB signalling from the Ingenuity Pathway Analysis (IPA) Software (Qiagen).

Statistical analysis

Results are presented as mean values ± s.d., with sample size and number of repeats indicated in the figure legends. One-way ANOVA with the multiple comparisons Bonferroni test was used to compare multiple groups. For comparisons between two groups, unpaired or paired two-tailed Student's t-test was used. P values less than 0.05 were considered significant. Analyses were conducted using GraphPad Prism 6 or 8 software (GraphPad Software).

Reporting summary

Further information on research design is available in the Nature Research Reporting Summary linked to this paper.

Data availability

Microarray data were submitted to the NCBI Gene Expression Omnibus (GEO) database (https://www.ncbi.nlm.nih.gov/geo/) accession number GSE125521. scRNA-seq data were submitted to the NCBI GEO database accession number GSE151674. scRNA-seq metadata can be found in Supplementary Table 4. Proteomics data can be found in Supplementary Table 5. Series matrix files were also downloaded from the NCBI GEO databases: GSE47460–GPL14550, GSE37768, GSE56768 and GSE52509. Proteomic peak lists were searched against the mouse Uniprot FASTA database (version November 2016) https://www.uniprot.org/proteomes/UP000000589. All other data supporting the findings of this study are available within the Article and Supplementary Information. All data are available from the corresponding authors upon reasonable request. Source data are provided with this paper.

Code availability

All code used for data visualization of the scRNA-seq data can be found at https://github.com/theislab/2020_Inhibition_LTbetaR-signalling.

36. Baarsma, H. A. et al. Noncanonical WNT-5A signaling impairs endogenous lung repair in COPD. *J. Exp. Med.* **214**, 143–163 (2017).
37. Barkauskas, C. E. et al. Type 2 alveolar cells are stem cells in adult lung. *J. Clin. Invest.* **123**, 3025–3036 (2013).
38. Ng-Blichfeldt, J. P. et al. Retinoic acid signaling balances adult distal lung epithelial progenitor cell growth and differentiation. *EBioMedicine* **36**, 461–474 (2018).
39. John, G. et al. The composition of cigarette smoke determines inflammatory cell recruitment to the lung in COPD mouse models. *Clin. Sci. (Lond.)* **126**, 207–221 (2014).
40. Yildirim, A. O. et al. Palifermin induces alveolar maintenance programs in emphysematous mice. *Am. J. Respir. Crit. Care Med.* **181**, 705–717 (2010).
41. Fuchs, H. et al. Mouse phenotyping. *Methods* **53**, 120–135 (2011).
42. Fallica, J., Das, S., Horton, M. & Mitzner, W. Application of carbon monoxide diffusing capacity in the mouse lung. *J. Appl. Physiol.* **110**, 1455–1459 (2011).
43. Strunz, M. et al. Longitudinal single cell transcriptomics reveals Krt8$^+$ alveolar epithelial progenitors in lung regeneration. Preprint at https://doi.org/10.1101/705244 (2019).
44. Angelidis, I. et al. An atlas of the aging lung mapped by single cell transcriptomics and deep tissue proteomics. *Nat. Commun.* **10**, 963 (2019).
45. Macosko, E. Z. et al. Highly parallel genome-wide expression profiling of individual cells using nanoliter droplets. *Cell* **161**, 1202–1214 (2015).
46. Hughes, T. K. et al. Highly efficient, massively-parallel single-cell RNA-seq reveals cellular states and molecular features of human skin pathology. Preprint at https://doi.org/10.1101/689273 (2019).
47. Wolf, F. A., Angerer, P. & Theis, F. J. SCANPY: large-scale single-cell gene expression data analysis. *Genome Biol.* **19**, 15 (2018).
48. Luecken, M. D. & Theis, F. J. Current best practices in single-cell RNA-seq analysis: a tutorial. *Mol. Syst. Biol.* **15**, e8746 (2019).
49. Lun, A. T., McCarthy, D. J. & Marioni, J. C. A step-by-step workflow for low-level analysis of single-cell RNA-seq data with Bioconductor. *F1000Res.* **5**, 2122 (2016).
50. Shevchenko, A., Tomas, H., Havlis, J., Olsen, J. V. & Mann, M. In-gel digestion for mass spectrometric characterization of proteins and proteomes. *Nat. Protoc.* **1**, 2856–2860 (2006).
51. Cox, J. & Mann, M. MaxQuant enables high peptide identification rates, individualized p.p.b.-range mass accuracies and proteome-wide protein quantification. *Nat. Biotechnol.* **26**, 1367–1372 (2008).
52. Schiller, H. B. et al. Deep proteome profiling reveals common prevalence of MZB1-positive plasma B cells in human lung and skin fibrosis. *Am. J. Respir. Crit. Care Med.* **196**, 1298–1310 (2017).
53. Tyanova, S. et al. The Perseus computational platform for comprehensive analysis of (prote)omics data. *Nat. Methods* **13**, 731–740 (2016).
54. Rainer, J., Sanchez-Cabo, F., Stocker, G., Sturn, A. & Trajanoski, Z. CARMAweb: comprehensive R- and bioconductor-based web service for microarray data analysis. *Nucleic Acids Res.* **34**, W498–W503 (2006).
55. Malehmir, M. et al. Platelet GPIbQα is a mediator and potential interventional target for NASH and subsequent liver cancer. *Nat. Med.* **25**, 641–655 (2019).
56. Wang, X., Spandidos, A., Wang, H. & Seed, B. PrimerBank: a PCR primer database for quantitative gene expression analysis, 2012 update. *Nucleic Acids Res.* **40**, D1144–D1149 (2012).
57. Gendusa, R., Scalia, C. R., Buscone, S. & Cattoretti, G. Elution of high-affinity (>10-9 KD) antibodies from tissue sections: clues to the molecular mechanism and use in sequential immunostaining. *J. Histochem. Cytochem.* **62**, 519–531 (2014).
58. Schindelin, J. et al. Fiji: an open-source platform for biological-image analysis. *Nat. Methods* **9**, 676–682 (2012).
59. Berg, S. et al. ilastik: interactive machine learning for (bio)image analysis. *Nat. Methods* **16**, 1226–1232 (2019).
60. Wählby, C. et al. An image analysis toolbox for high-throughput *C. elegans* assays. *Nat. Methods* **9**, 714–716 (2012).

Article

61. John-Schuster, G. et al. Cigarette smoke-induced iBALT mediates macrophage activation in a B cell-dependent manner in COPD. *Am. J. Physiol. Lung Cell. Mol. Physiol.* **307**, L692–L706 (2014).
62. Jenkins, R. G. et al. An official american thoracic society workshop report: use of animal models for the preclinical assessment of potential therapies for pulmonary fibrosis. *Am. J. Respir. Cell Mol. Biol.* **56**, 667–679 (2017).
63. Corti, M., Brody, A. R. & Harrison, J. H. Isolation and primary culture of murine alveolar type II cells. *Am. J. Respir. Cell Mol. Biol.* **14**, 309–315 (1996).
64. Königshoff, M. et al. WNT1-inducible signaling protein-1 mediates pulmonary fibrosis in mice and is upregulated in humans with idiopathic pulmonary fibrosis. *J. Clin. Invest.* **119**, 772–787 (2009).
65. Mutze, K., Vierkotten, S., Milosevic, J., Eickelberg, O. & Königshoff, M. Enolase 1 (ENO1) and protein disulfide-isomerase associated 3 (PDIA3) regulate Wnt/β-catenin-driven trans-differentiation of murine alveolar epithelial cells. *Dis. Model. Mech.* **8**, 877–890 (2015).
66. Lehmann, M. et al. Senolytic drugs target alveolar epithelial cell function and attenuate experimental lung fibrosis *ex vivo*. *Eur. Respir. J.* **50**, 1602367 (2017).
67. Caporale, A., Tartaggia, S., Castellin, A. & De Lucchi, O. Practical synthesis of aryl-2-methyl-3-butyn-2-ols from aryl bromides via conventional and decarboxylative copper-free Sonogashira coupling reactions. *Beilstein J. Org. Chem.* **10**, 384–393 (2014).
68. Veeman, M. T., Slusarski, D. C., Kaykas, A., Louie, S. H. & Moon, R. T. Zebrafish prickle, a modulator of noncanonical Wnt/Fz signaling, regulates gastrulation movements. *Curr. Biol.* **13**, 680–685 (2003).
69. Mootha, V. K. et al. PGC-1α-responsive genes involved in oxidative phosphorylation are coordinately downregulated in human diabetes. *Nat. Genet.* **34**, 267–273 (2003).
70. Subramanian, A. et al. Gene set enrichment analysis: a knowledge-based approach for interpreting genome-wide expression profiles. *Proc. Natl Acad. Sci. USA* **102**, 15545–15550 (2005).
71. Kim, S. et al. Integrative phenotyping framework (iPF): integrative clustering of multiple omics data identifies novel lung disease subphenotypes. *BMC Genomics* **16**, 924 (2015).

Author contributions T.M.C., G.J.S., O.E., M.K., M.H. and A.Ö.Y. conceived the study and experimental design. T.M.C., G.J.S., D.H., M.A.L., R.C., Y.H., Z.E., C.C., S.P., J.H., H.A., G.G., M.Z.J., L.B., D.P., M.S.K., A.G., A.J., G. Beroshvili, M.C.F., M.D., I.S., J.J. and D.W. performed experiments. M.H., F.T., D.P. and M.S.K. designed, undertook, and analysed flow cytometry experiments. A.G. designed, undertook, and analysed multiplex immunofluorescence, supervised by F.T. E.G. and B.P. prepared NIK inhibitor. S.E.V. prepared patient lung core samples. M.I. and J.B. contributed to microarray analysis. M.H., D.H. designed and executed the immunohistochemistry and RNA in situ hybridization analyses. M.H.dA. supervised microarray analyses. M.A., M.S. and I.A. designed, undertook, and analysed scRNA-seq experiments, supervised by H.B.S. and F.J.T. I.S. undertook proteomics analysis. C.M. analysed proteomic datasets. M. Lindner supplied human lung tissue for lung slices. D.W. and M.K. established the 3D human lung slice model. Y.H., C.C. and M.K. developed and undertook human lung organoid experiments. T.M.C., G.J.S., D.P., M. Lehmann, M.A., M.S., I.A., C.M., Y.H., T.S., P.K., C.C., G. Burgstaller, R.G., R.C., M.S.K., A.G., M.C.F., F.J.T., F.T., M.B., E.D., H.B.S., M.K., M.H. and A.Ö.Y. analysed and interpreted data. T.M.C., G.J.S., T.O.C., M.H. and A.Ö.Y. wrote the manuscript. All authors read and edited the manuscript.

Competing interests G.J.S. is currently employed as an editor at *Genome Medicine*, a Springer Nature journal. He joined the company after his participation in the study and was not involved in the editorial process at *Nature*. All other authors declare no competing interests.
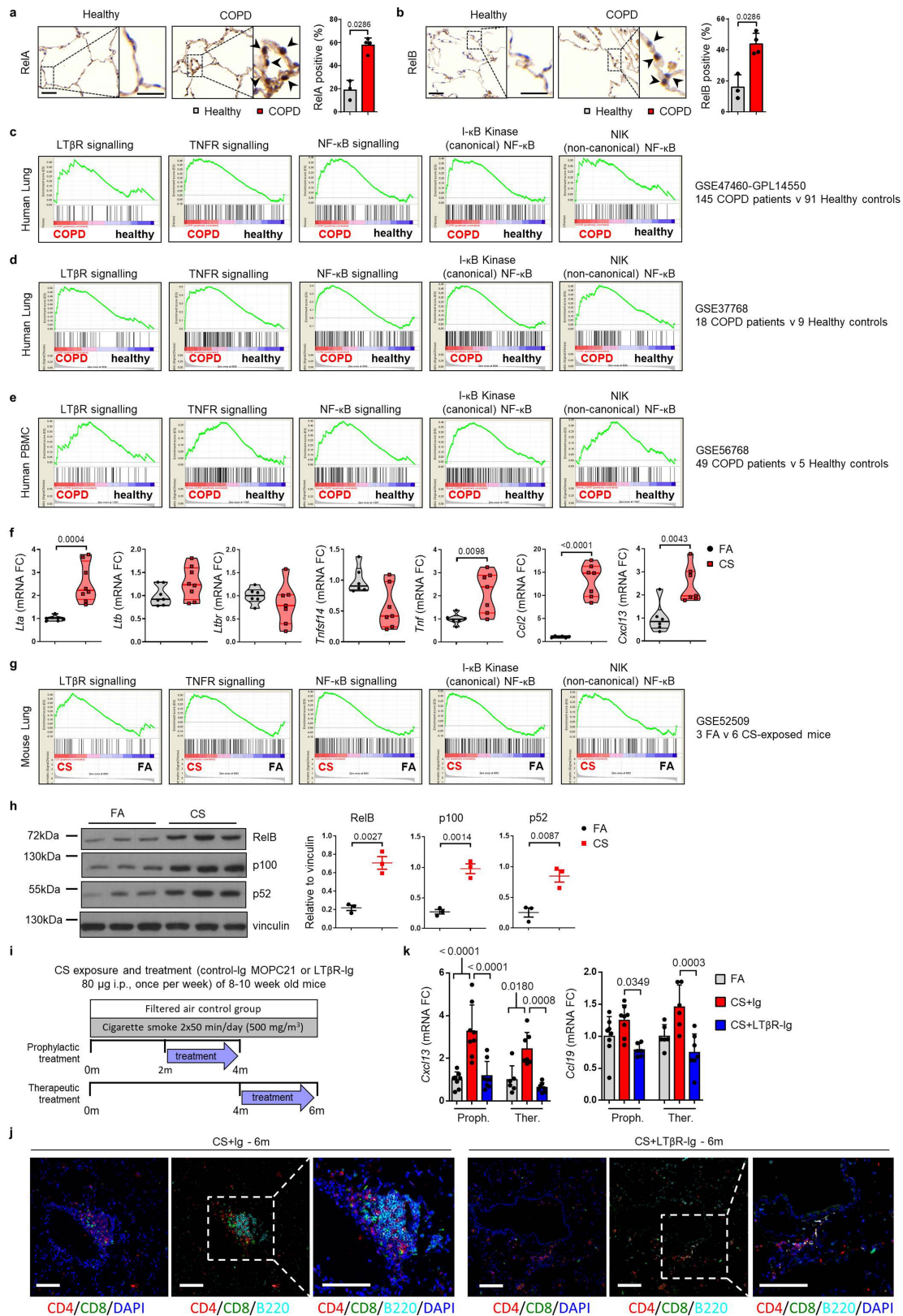
Additional information
Supplementary information is available for this paper at https://doi.org/10.1038/s41586-020-2882-8.
Correspondence and requests for materials should be addressed to M.H. or A.Ö.Y.
Peer review information *Nature* thanks the anonymous reviewers for their contribution to the peer review of this work.
**Reprints and permissions information** is available at http://www.nature.com/reprints.

a

RelA — Healthy — COPD

RelA positive (%) 0.0286

□ Healthy ■ COPD

b

RelB — Healthy — COPD

RelB positive (%) 0.0286

□ Healthy ■ COPD

c

Human Lung

LTβR signalling | TNFR signalling | NF-κB signalling | I-κB Kinase (canonical) NF-κB | NIK (non-canonical) NF-κB

COPD healthy

GSE47460-GPL14550
145 COPD patients v 91 Healthy controls

d

Human Lung

LTβR signalling | TNFR signalling | NF-κB signalling | I-κB Kinase (canonical) NF-κB | NIK (non-canonical) NF-κB

COPD healthy

GSE37768
18 COPD patients v 9 Healthy controls

e

Human PBMC

LTβR signalling | TNFR signalling | NF-κB signalling | I-κB Kinase (canonical) NF-κB | NIK (non-canonical) NF-κB

COPD healthy

GSE56768
49 COPD patients v 5 Healthy controls

f

Lta (mRNA FC) 0.0004 | *Ltb* (mRNA FC) | *Ltbr* (mRNA FC) | *Tnfsf14* (mRNA FC) | *Tnf* (mRNA FC) 0.0098 | *Ccl2* (mRNA FC) <0.0001 | *Cxcl13* (mRNA FC) 0.0043

● FA ■ CS

g

Mouse Lung

LTβR signalling | TNFR signalling | NF-κB signalling | I-κB Kinase (canonical) NF-κB | NIK (non-canonical) NF-κB

CS FA

GSE52509
3 FA v 6 CS-exposed mice

h

FA — CS

72kDa — RelB
130kDa — p100
55kDa — p52
130kDa — vinculin

RelB 0.0027 | p100 0.0014 | p52 0.0087

Relative to vinculin

● FA ■ CS

i

CS exposure and treatment (control-Ig MOPC21 or LTβR-Ig 80 μg i.p., once per week) of 8-10 week old mice

Filtered air control group
Cigarette smoke 2x50 min/day (500 mg/m³)

Prophylactic treatment
0m — 2m — treatment — 4m

Therapeutic treatment
0m — 4m — treatment — 6m

k

Cxcl13 (mRNA FC)
<0.0001
<0.0001
0.0180
0.0008
Proph. | Ther.

Ccl19 (mRNA FC)
0.0349
0.0003
Proph. | Ther.

□ FA ■ CS+Ig ■ CS+LTβR-Ig

j

CS+Ig - 6m

CD4/CD8/DAPI | CD4/CD8/B220 | CD4/CD8/B220/DAPI

CS+LTβR-Ig - 6m

CD4/CD8/DAPI | CD4/CD8/B220 | CD4/CD8/B220/DAPI

Extended Data Fig. 1 | See next page for caption.

Article

Extended Data Fig. 1 | Canonical and non-canonical NF-κB signalling pathways are activated in the lungs of patients with COPD and mice exposed to cigarette smoke. a, **b**, Representative images of immunohistochemical analysis for RELA (**a**) and RELB (**b**) (brown signal, indicated by arrows, nuclei counterstained with haematoxylin) in lung core biopsy sections from healthy participants (*n* = 3) patients with COPD (*n* = 4), with the quantification of RELA and RELB-positive alveolar epithelial nuclei shown as mean ± s.d. Scale bar, 50 μm and 25 μm (inset). **c**–**e**, GSEA of the LTβR signalling, NF-κB signalling (gene lists from IPA software, Qiagen), TNFR-mediated signalling (GO:0033209), positive regulation of I-κB kinase NF-κB signalling (GO:0043123) and NIK NF-κB signalling (GO:0038061) pathways in publicly available array data from lung tissue (GSE47460–GPL14550) of healthy (*n* = 91) versus patients with COPD (*n* = 145) (**c**), from lung tissue (GSE37768) of healthy (*n* = 9) versus patients with COPD (*n* = 18) (**d**) and from PBMCs (GSE56768) of healthy (*n* = 5) versus patients with COPD (*n* = 49) (**e**). **f**, mRNA expression levels of *Lta*, *Ltbr*, *Tnfsf14*, *Tnf*, *Ccl2* and *Cxcl13* determined by qPCR in whole lung from B6 mice exposed to filtered air (*n* = 6) or cigarette smoke (*n* = 8) for 6 months; individual mice are shown. **g**, GSEA of the pathways described in **c**–**e** in the publicly available array data (GSE52509) of lungs from our mice exposed to filtered air (*n* = 3) and cigarette smoke (*n* = 6) for 4 and 6 months. **h**, Western blot analysis for RELB, p100 and p52 in total lung homogenate from the mice described in **f**. Quantification relative to vinculin of individual mice shown (*n* = 3). For gel source data, see Supplementary Fig. 1. **i**, Schematic representation of the LTβR–Ig treatment protocol. **j**, Representative low and high magnification overlay images of Multiplex immunofluorescence staining to identify CD4 (red), CD8 (green), B220 (turquoise) and DAPI (blue) counterstained lung sections (*n* = 4) from B6 mice exposed to cigarette smoke for 6 months, plus LTβR–Ig fusion protein or control Ig (80 μg intraperitoneally, weekly) therapeutically from 4 to 6 months, and analysed at 6 months. Scale bars, 100 μm **k**, mRNA expression levels of *Cxcl13* and *Ccl19* determined by qPCR in whole lung from B6 mice exposed to filtered air or cigarette smoke for 4 and 6 months, plus LTβR–Ig fusion or control Ig (80 μg intraperitoneally, weekly) prophylactically from 2 to 4 months and analysed at 4 months, and therapeutically from 4 to 6 months and analysed at 6m (*n* = 4 mice/group, repeated twice, pooled data shown). *P* values indicated, Mann–Whitney one-sided test (**a**, **b**), unpaired two-tailed Student's *t*-test (**f**, **h**), one-way ANOVA multiple comparisons Bonferroni test (**k**).
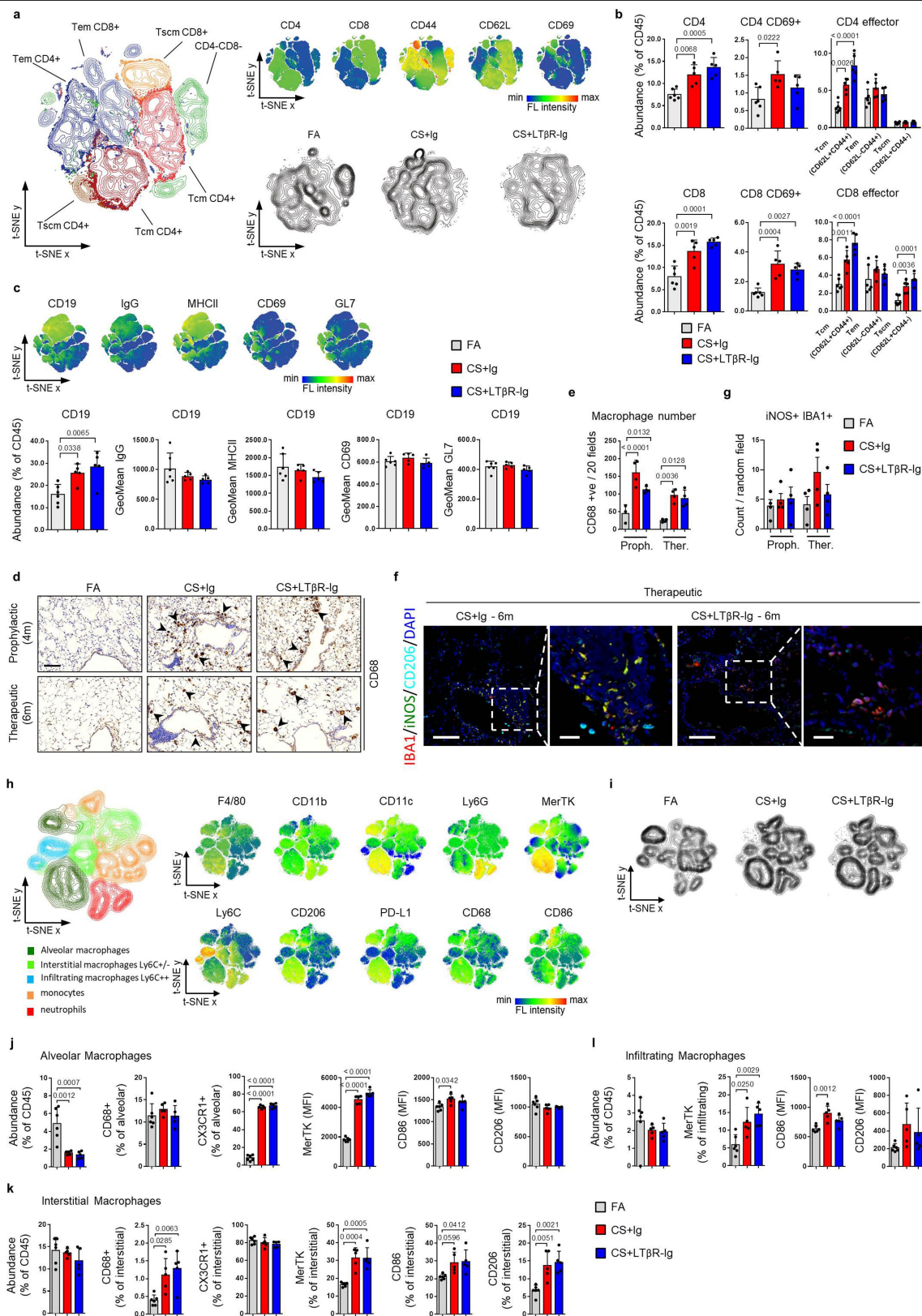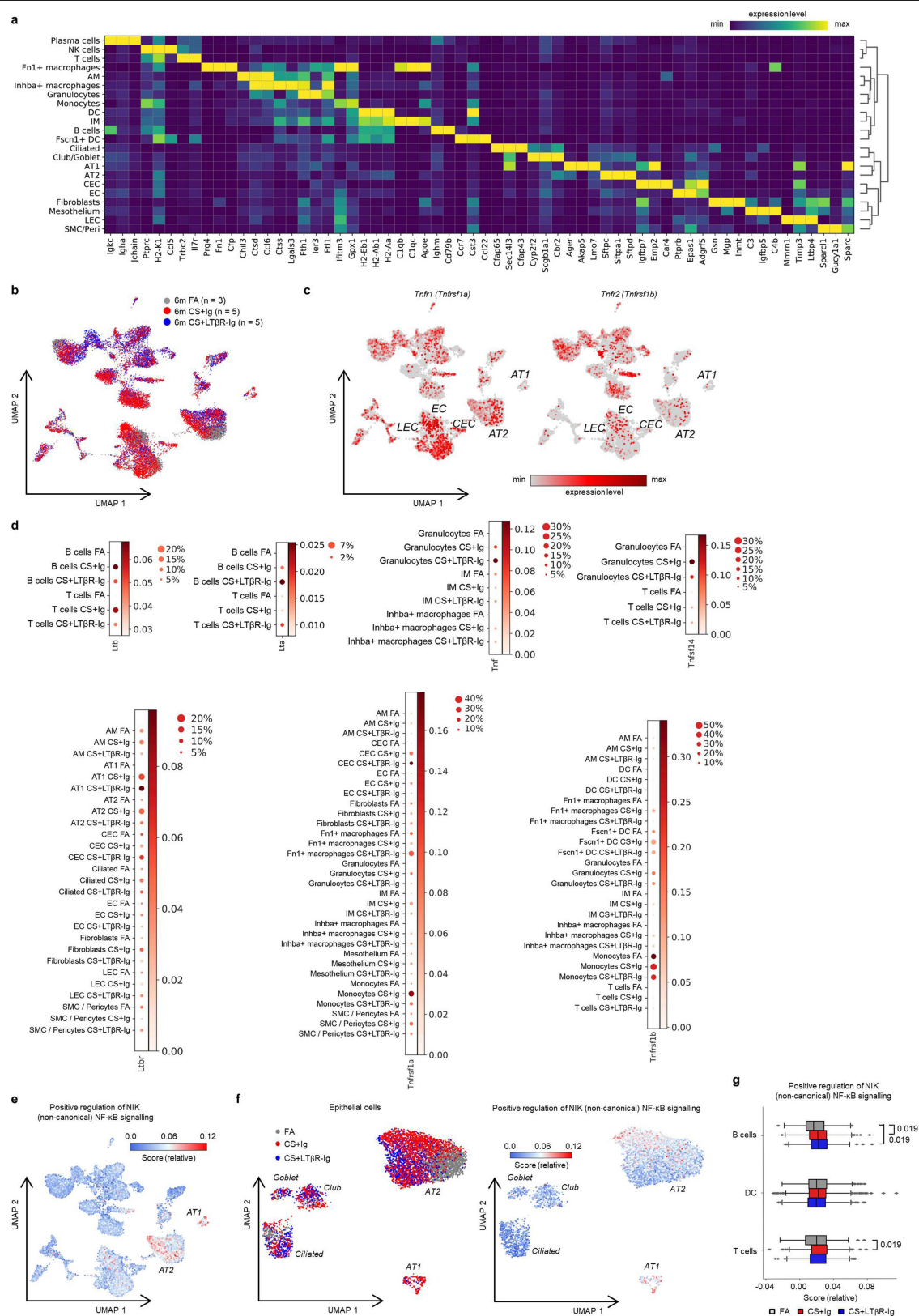
Extended Data Fig. 2 | See next page for caption.

Article

Extended Data Fig. 2 | Immune response in lungs of mice exposed to cigarette smoke and treated with LTβR–Ig. a–**c**, Flow cytometry analysis of single cell suspensions for adaptive immune cells from whole lung of B6 mice exposed to filtered air ($n = 6$) or cigarette smoke for 6 months, plus LTβR–Ig fusion ($n = 5$) or control Ig ($n = 5$) (80 µg intraperitoneally, weekly) from 4 to 6 months and analysed at 6 months. **a**, *t*-SNE plots showing the distribution and composition of CD4 and CD8 T cells as central memory T cells (Tcm) (CD62L⁺CD44⁺), effector memory T cells (Tem) (CD62L⁻CD44⁺) and T memory stem cells (Tscm) (CD62L⁺CD44⁻) (left) and *t*-SNE plots showing the distribution of the surface markers indicated (top right) and global changes in composition with treatment (bottom right). **b**, Abundance of the T cell populations indicated as a percentage of total CD45⁺ cells. **c**, Top, *t*-SNE plots showing the distribution of CD19-, IgG-, MHCII-, CD69- and GL7-positive cells. Bottom, the abundance of CD19⁺ B cells as a percentage of total CD45⁺ cells and the geometric mean fluorescence intensity of the expressed markers indicated on CD19⁺ B cells. **d**–**g**, B6 mice were exposed to filtered air or cigarette smoke for 4 and 6 months, plus LTβR–Ig fusion protein or control Ig (80 µg i.p., weekly) prophylactically (Proph.) from 2 to 4 months and analysed at 4 months and therapeutically (Ther.) from 4 to 6 months, and analysed at 6 months. **d**, Representative images of immunohistochemical analysis for CD68 macrophages in lung sections from the mice ($n = 4$ mice per group, brown

signal indicated by arrowheads, haematoxylin counter stained). Scale bar, 100 µm. **e**, Quantification of CD68 positive macrophages across 20 random fields of view from lung sections stained in **d** ($n = 4$ mice per group). **f**, Representative low and high magnification overlay images of Multiplex immunofluorescence staining to identify IBA1 (red), iNOS (green), CD206 (turquoise) and DAPI (blue) counterstained lung sections from mice at 6 months ($n = 4$ mice per group). Scale bars, 100 µm and 25 µm, respectively. **g**, iNOS and IBA1 double-positive macrophages from Multiplex immunofluorescence staining on lung sections from mice treated both prophylactically and therapeutically was quantified using Ilastik and CellProfiler ($n = 4$ mice per group). **h**–**l**, Flow cytometry analysis of single cell suspensions for myeloid cells from whole lung of B6 mice exposed to filtered air ($n = 6$) or cigarette smoke for 6 months, plus LTβR–Ig fusion ($n = 5$) or control Ig ($n = 5$) (80 µg intraperitoneally, weekly) from 4 to 6 months and analysed at 6 months. **h**, *t*-SNE plots showing the distribution and composition of myeloid cells and surface markers indicated. **i**, *t*-SNE plots showing global changes in composition with treatment. **j**, Composition of CD45⁺LY6G⁻F480⁺CD11c⁺ alveolar macrophages. **k**, Composition of CD45⁺LY6G⁻F480⁺CD11c⁻CD11b⁺ interstitial macrophages. **l**, Composition of CD45⁺LY6G⁻F480⁺CD11c⁻CD11b⁺LY 6C^high infiltrating macrophages. Data are mean ± s.d. *P* values determined by one-way ANOVA multiple comparisons Bonferroni test (**b**, **c**, **e**, **g**, **j**–**l**).

Extended Data Fig. 3 | See next page for caption.

Article

Extended Data Fig. 3 | scRNA-seq analysis of lungs from mice exposed to cigarette smoke and treated with LTβR–Ig. Cells from whole lung suspensions of B6 mice exposed to filtered air ($n = 3$) or cigarette smoke for 6 months, plus LTβR–Ig fusion protein ($n = 5$) or control Ig ($n = 5$) therapeutically from 4 to 6 months, were analysed at 6 months by scRNA-seq (Drop-Seq). **a**, Heat map depicting the expression of key genes used in identifying the individual cell populations. **b**, UMAP of scRNA-seq profiles (dots) coloured by experimental group. **c**, UMAP plots showing expression of genes indicated in scRNA-seq profiles. **d**, Dot blot depicting the expression level (log-transformed, normalized UMI counts) and percentage of cells in a population positive for *Ltb*, *Lta*, *Tnf*, *Tnfsf14*, *Ltbr*, *Tnfrsf1a* and *Tnfrsf1b*. **e**, UMAP plot showing the relative intensity of the positive regulation of NIK (non-canonical) NF-κB signalling pathway (GO:1901224) across the scRNA-seq profiles. **f**, UMAP plot of scRNA-seq profiles (dots) of lung epithelial cells coloured by experimental group (left) and the relative intensity of the positive regulation of NIK (non-canonical) NF-κB signalling pathway (GO:1901224) (right). **g**, Box and whiskers plot (box representing 25th–75th percentile, median line indicated and Tukey whiskers representing ±1.5× IQR) showing the relative score for the positive regulation of NIK (non-canonical) NF-κB signalling pathway in the cell types indicated across the three groups. Statistical significance was assessed using Wilcoxon rank-sum two-sided test on normalized, log-transformed count values and corrected with Benjamini–Hochberg.
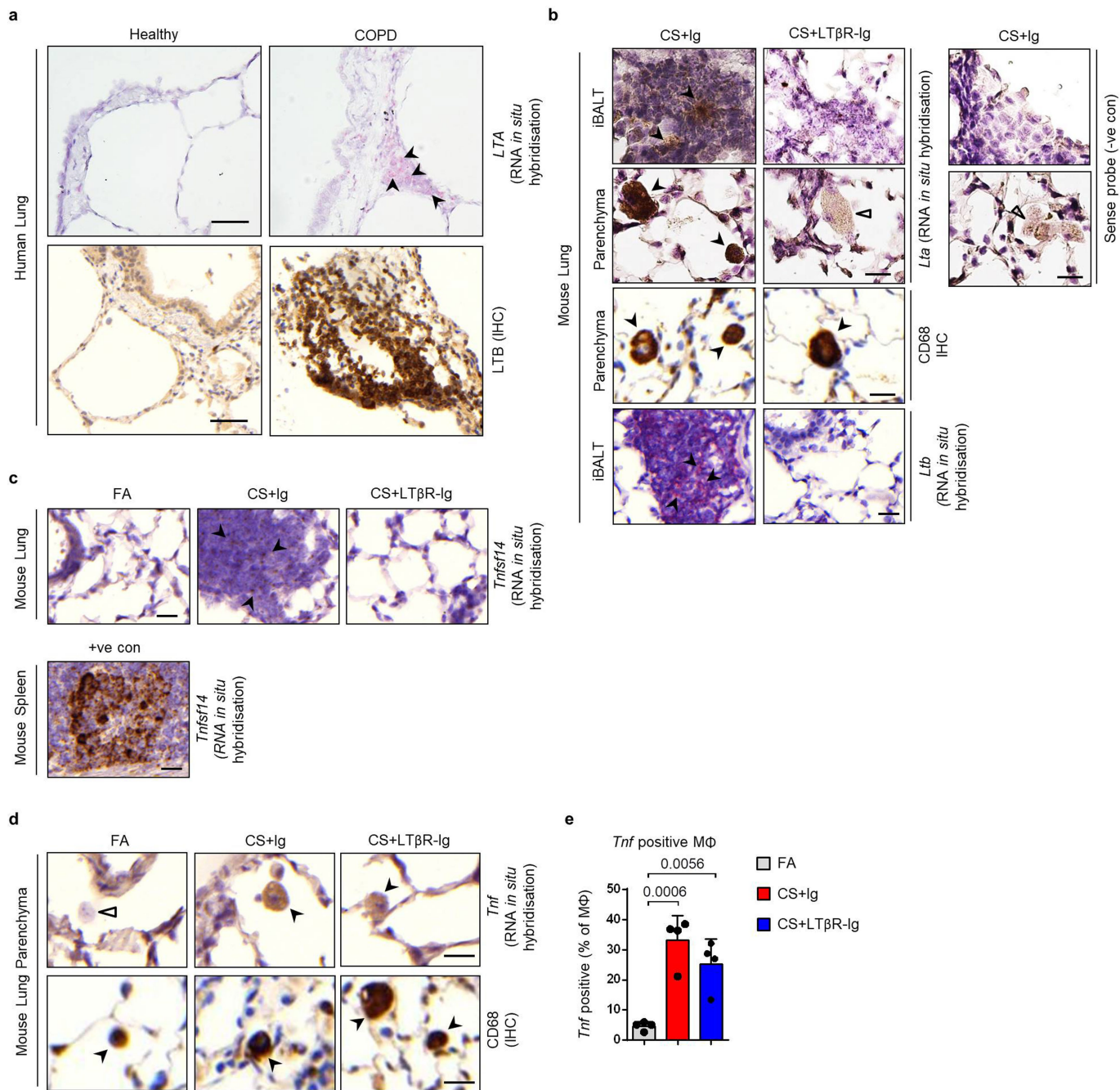
Extended Data Fig. 4 | Analysis of LTA and LTB expression in human and mouse lungs. a, Representative images of in situ hybridization analysis for *LTA* and immunohistochemical analysis for LTB in lung sections from healthy participants and patients with COPD (*n* = 4, red signal indicated by arrowheads (*LTA*), brown signal (LTB) and nuclei counterstained with haematoxylin). Scale bar, 50 μm. **b**, Representative images of in situ hybridization analysis for *Lta* and *Ltb* in lung sections from B6 mice exposed to cigarette smoke for 6 months with LTβR–Ig fusion protein or control Ig (80 μg intraperitoneally, weekly) therapeutically for 4 to 6 months, and analysed at 6 months (brown positive staining (*Lta*) and red positive staining (*Ltb*) indicated by arrowheads, open arrowhead unstained cells, nuclei were counterstained with haematoxylin) (*n* = 4 mice per group, repeated twice). Scale bar, 20 μm. Non-staining with sense probe in cigarette smoke plus Ig sections shown as negative control. Representative images of immunohistochemical analysis identifying

CD68-positive macrophages (brown staining indicated by arrowheads) also shown. **c**, Representative images of in situ hybridization analysis for *Tnfsf14* in lung sections from mice described in **b** (brown positive staining indicated by arrowheads, open arrowhead unstained cells, nuclei counterstained with haematoxylin) (*n* = 4 mice per group). Scale bars, 20 μm. Spleen section shown as a positive control. **d**, Representative images of in situ hybridization analysis for *Tnf* in lung sections from mice described in **b** (brown positive macrophage indicated by arrowheads, open arrowhead unstained macrophage, nuclei counterstained with haematoxylin). Scale bars, 20 μm. Representative immunohistochemical analysis identifying CD68-positive macrophages (brown staining indicated by arrowheads, haematoxylin counterstained) also shown. Scale bars, 20 μm. **e**, Quantification of *Tnf*-positive macrophages across 20 random fields of view per lung (*n* = 4). Data are mean ± s.d. *P* values determined by one-way ANOVA multiple comparisons Bonferroni test.

Article

Extended Data Fig. 5 | See next page for caption.

Extended Data Fig. 5 | Inhibition of LTβR signalling strongly reduces non-canonical but not canonical NF-κB signalling in lung. a, Principal component analysis of microarray data, using Mouse Ref-8 v2.0 Expression BeadChips (Illumina), performed on lung tissue from mice exposed to filtered air or cigarette smoke for 6 months, plus LTβR–Ig fusion or control Ig (80 μg intraperitoneally, weekly) therapeutically from 4 to 6 months ($n = 3$ mice per group). **b**, Principal component analysis of normalized z-scored mass spectrometry intensities from proteomics of whole lung lysates from mice exposed to filtered air ($n = 6$) or cigarette smoke for 6 months, plus LTβR–Ig fusion ($n = 7$) or control Ig ($n = 4$) (80 μg intraperitoneally, weekly) from 4 to 6 months. **c**, Heat map depicting the top 20 up and down LTβR–Ig regulated genes presented as fold change (FDR < 10%) from the microarray data described in **a**. Left, expression in mice exposed to cigarette smoke plus Ig relative to mice exposed to filtered air. Right, expression in mice exposed to cigarette smoke plus LTβR–Ig relative to mice exposed to cigarette smoke plus Ig. **d**, GSEA of the NIK (non-canonical) NF-κB signalling (GO:0038061) pathway of the microarray data from **a**. **e**, Heat map of significantly regulated proteins from the NIK (non-canonical) NF-κB signalling (GO:0038061) pathway as determined by Student's t-test statistic from the proteomics data described in **b**. **f**, GSEA of the NIK (non-canonical) NF-κB signalling (GO:0038061) pathway of the normalized proteome data described in **b**. **g**, Representative images of two independent experiments of immunohistochemical analysis for RELB in lung sections from B6 mice exposed to filtered air or cigarette smoke for 4 or 6 months, plus LTβR–Ig fusion or control Ig (80 μg intraperitoneally, weekly) prophylactically from 2 to 4 months and analysed at 4 months, and therapeutically from 4 to 6 months and analysed at 6 months (brown signal indicated by arrowheads, nuclei counterstained with haematoxylin). Scale bar, 25 μm. **h**, Quantification of RELB-positive alveolar epithelial nuclei from the immunohistochemistry sections in **g** ($n = 3$ mice per group). **i**, Representative images of two independent experiments of immunohistochemical analysis for RELA in lung sections from the mice described in **g** (brown signal indicated by arrowheads, nuclei counterstained with haematoxylin). Scale bar, 25 μm. **j**, Quantification of RELA-positive alveolar epithelial nuclei from the immunohistochemistry sections in **i** ($n = 3$ mice per group). **k**, mRNA expression levels of *Ccl2*, *Ccl3*, *Cxcl1* and *Tnf* determined by qPCR in whole lung from the mice described in **g** ($n = 4$ mice per group, repeated twice, pooled data shown). **l**, mRNA expression levels of *LTA*, *CXCL13* and *TNF* determined by qPCR in ex vivo human precision-cut lung slices stimulated for 24 h with LPS (10 μg ml^{-1}) in the presence or absence of human LTβR–Ig fusion protein (1 μg ml^{-1}) ($n = 3$ independent experiments from three separate lungs). Left image shows a representative picture of preparing a lung slice from the three independent experiments. Data are mean ± s.d. P values determined by one-way ANOVA multiple comparisons Bonferroni test.
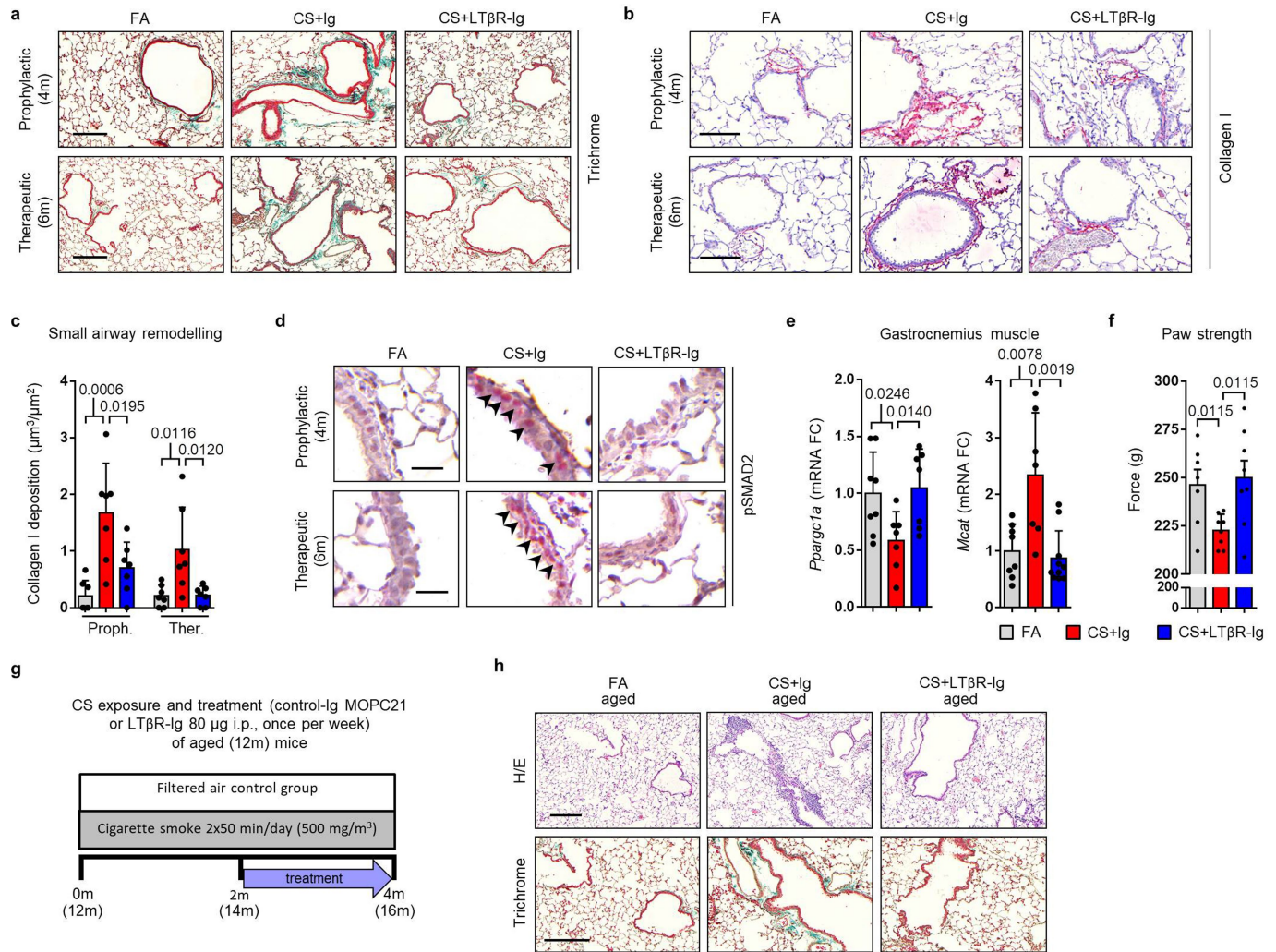
Extended Data Fig. 6 | LTβR–Ig treatment reverses airway remodelling and comorbidities in mice chronically exposed to cigarette smoke.
a, Representative images of Masson's Trichrome stained lung sections from B6 mice exposed to filtered air or cigarette smoke for 4 or 6 months, plus LTβR–Ig fusion protein or control Ig (80 μg intraperitoneally, weekly) prophylactically from 2 to 4 months and analysed at 4 months, and therapeutically from 4 to 6 months and analysed at 6 months (n = 4 mice per group, repeated twice). Scale bar, 200 μm. These are low-magnification images of the sections depicted and quantified in Fig. 2c, d. **b**, Representative images of immunohistochemical analysis for collagen I (red signal, nuclei counterstained with haematoxylin) in lung sections from B6 mice described in **a**. Scale bar, 100 μm. **c**, Quantification of small airway collagen deposition normalized to the surface area of airway and vessel basement membrane from the sections in **b** (n = 7 mice FA, 7 mice CS+Ig, 7 mice CS+LTβR-Ig groups, from two independent experiments). **d**, Representative images of immunohistochemical analysis for phosphorylated SMAD2 in lung sections from mice described in **a**

(red signal indicated by arrows, nuclei counterstained with haematoxylin) (n = 4 mice per group, repeated twice). Scale bar, 25 μm. **e**, mRNA expression levels of *Ppargc1a* and *Mcat* determined by qPCR in gastrocnemius muscle from 6-month mice described in **a** (n = 4 mice per group, repeated twice, pooled data shown). **f**, Four-paw muscle strength test in mice at 6 months treated as described in **a** (n = 8 mice per group). **g**, Schematic representation of the LTβR–Ig treatment protocol in aged mice. **h**, Representative images of lung sections stained with H&E and Masson's Trichrome from 12-month-old B6 mice exposed to filtered air or cigarette smoke for 4 months, plus LTβR–Ig fusion protein or control Ig (80 μg i.p., weekly) from 2 to 4 months and analysed at 4 months (n = 5 mice FA, 5 mice CS+Ig, 7/8 mice CS+LTβR-Ig groups, repeated twice). Scale bar, 50 μm. These are low magnification images of the sections depicted and quantified in Fig. 2f, g.) Data are mean ± s.d. P values determined by one-way ANOVA multiple comparisons Bonferroni test (**c**) or Student's two-tailed t-test (**e**, **f**).
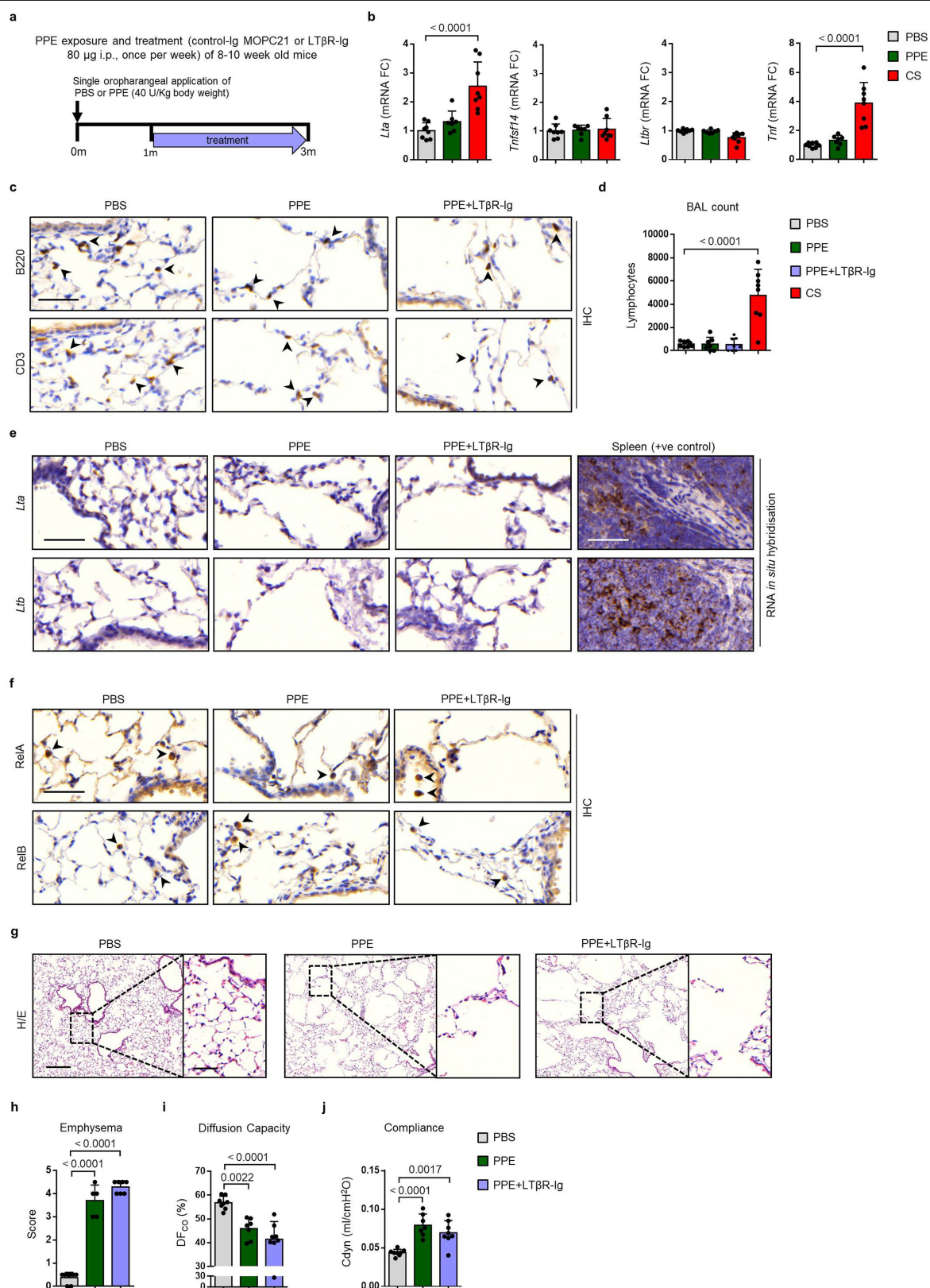
Extended Data Fig. 7 | See next page for caption.

Article

Extended Data Fig. 7 | Disease development is not attenuated by LTβR–Ig treatment in iBALT independent emphysema. a, Schematic representation of the LTβR–Ig treatment protocol in mice exposed to a single oropharangeal application of PPE or PBS control. **b**, mRNA expression level fold changes (FC) of *Lta*, *Tnfsf14*, *Ltbr* and *Tnf* relative to *Hprt*, determined by qPCR in whole lung from B6 mice treated with a single oropharyngeal application of PBS (*n* = 8) or PPE (40 U kg^{-1} body weight) and analysed after 3 months (*n* = 7) or 4 months of chronic exposure to cigarette smoke (*n* = 8 mice per group). **c**, Representative images of immunohistochemical analysis for B220-positive B cells and CD3-positive T cells (brown signal, indicated by arrowheads, nuclei counterstained with haematoxylin) in lung sections from mice treated with PBS or PPE as described in **b**, plus mice treated with PPE followed by LTβR–Ig fusion protein (80 μg intraperitoneally, weekly) 28 days later for 2 months (*n* = 8 mice per group, repeated twice). Scale bar, 50 μm. **d**, Lymphocyte counts in the BAL fluid from the mice described in **c** plus mice exposed to cigarette smoke for 4 months (*n* = 8 mice per group). **e**, Representative images of in situ hybridization analysis for *Lta* and *Ltb* in lung sections from mice described in **c**, plus splenic positive controls (brown staining, nuclei counterstained with haematoxylin) (*n* = 4 mice per group, repeated twice). Scale bar, 50 μm. **f**, Representative images of immunohistochemical analysis for RELA and RELB in lung sections from B6 mice described in **c** (brown signal indicated by arrowheads, nuclei counterstained with haematoxylin) (*n* = 4 mice per group, repeated twice). Scale bar, 50 μm. **g**, Representative images of H&E-stained lung sections from mice described in **c** (*n* = 8 mice per group, repeated twice). Scale bars, 200 μm and 50 μm (inset). **h**, Emphysema scoring (1–5; 5 most severe) of lung sections from **f** (*n* = 5 mice PBS, 5 mice PPE, 7 mice PPE+LTβR-Ig groups). **i**, Diffusing capacity of carbon monoxide (DF$_{CO}$) in the lungs of mice described in **c** (*n* = 8 mice PBS, 7 mice PPE, 8 mice PPE+LTβR-Ig groups). **j**, Dynamic compliance (Cdyn) pulmonary function data from the mice described in **c** (*n* = 8 mice PBS, 7 mice PPE, 8 mice PPE+LTβR-Ig groups). Data are mean ± s.d. *P* values determined by one-way ANOVA multiple comparisons Bonferroni test.
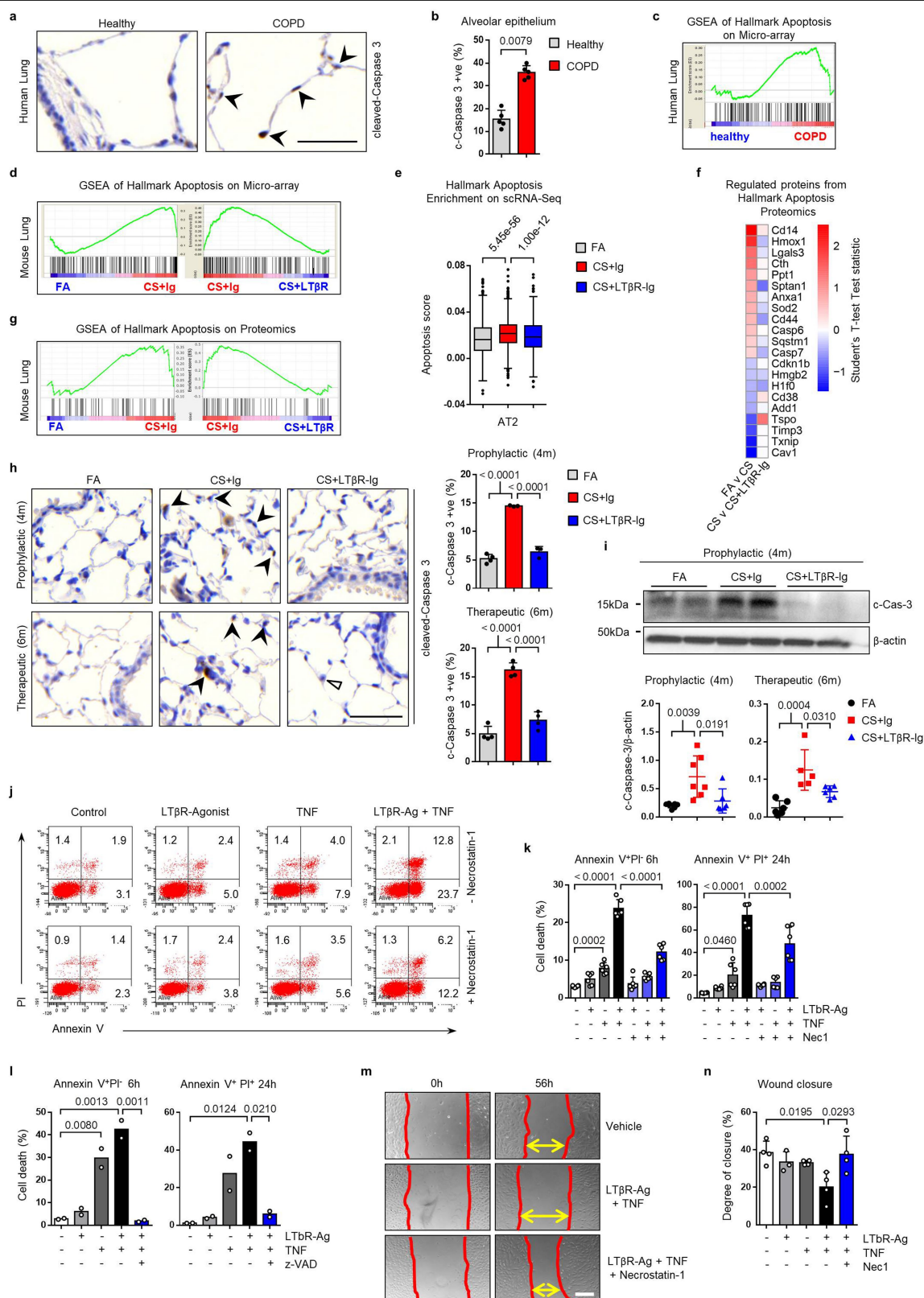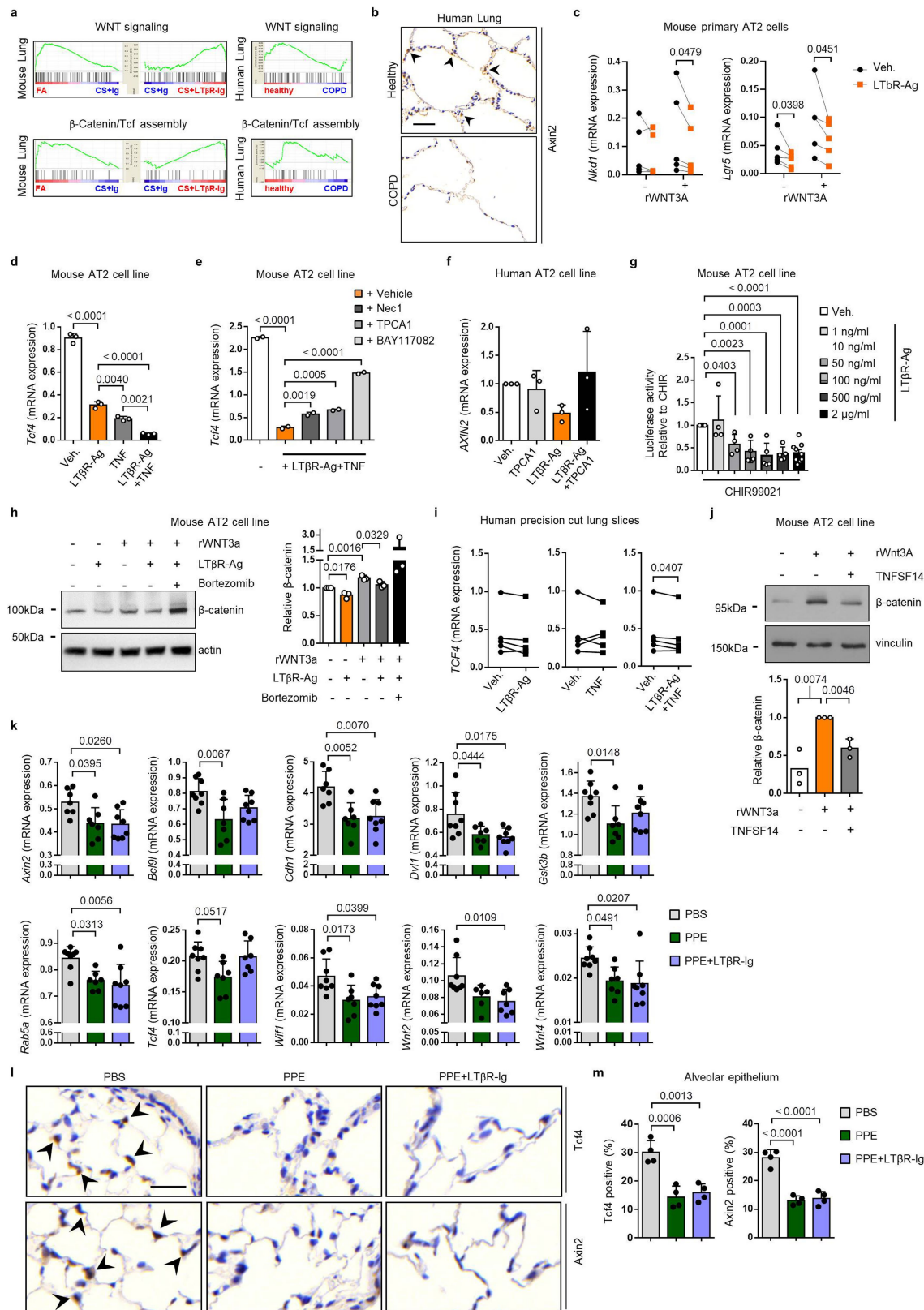
Extended Data Fig. 8 | See next page for caption.

Article

Extended Data Fig. 8 | Inhibiting LTβR-signalling suppresses cigarette-smoke-induced apoptosis. a, Representative images of immunohistochemical analysis for cleaved caspase-3 in lung sections from healthy participants and patients with COPD ($n = 5$, brown signal indicated by arrowheads, nuclei counterstained with haematoxylin). Scale bar, 50 μm. **b**, Quantification of alveolar epithelial cells positive for cleaved caspase-3 from the lung sections stained in **a**. Data are mean ± s.d. ($n = 5$ patients per group). $P = 0.0079$, Mann–Whitney two-sided test. **c, d**, GSEA of apoptosis (Hallmark collection) in transcriptomic array data from publicly available array data of lung tissue (GSE47460–GPL14550) from healthy participants ($n = 91$) versus patients with COPD ($n = 145$) (**c**) and the lungs of B6 mice after exposure for 6 months to filtered air, cigarette smoke plus Ig, or cigarette smoke plus LTβR–Ig fusion protein therapeutically ($n = 3$ mice per group) (**d**). **e**, Box and whiskers plot (box representing 25th–75th percentile, median line indicated and Tukey whiskers representing ±1.5 × IQR) showing the relative score for apoptosis (Hallmark collection) in AT2 cells after scRNA-seq analysis of lungs from B6 mice after exposure for 6 months to filtered air ($n = 3$ mice per group), cigarette smoke plus Ig ($n = 5$ mice per group) or cigarette smoke plus LTβR–Ig fusion protein ($n = 5$ mice per group) therapeutically. Statistical significance was determined by Wilcoxon rank-sum two-sided test on normalized, log-transformed count values and corrected with Benjamini–Hochberg. **f, g**, Proteome analysis of whole lung lysates from mice exposed to filtered air ($n = 6$) or cigarette smoke for 6 months, plus LTβR–Ig fusion ($n = 7$) or control Ig ($n = 4$) (80 μg intraperitoneally, weekly) from 4 to 6 months was undertaken. **f**, Heat map of the significantly regulated proteins from the Hallmark apoptosis list as determined by Student's two-sided t-test. **g**, GSEA of the Hallmark apoptosis list on the normalized proteome data. **h**, Representative images of immunohistochemical analysis for cleaved caspase-3 in lung sections from B6 mice exposed to filtered air or cigarette smoke for 4 and 6 months, plus LTβR–Ig fusion protein or control Ig (80 μg intraperitoneally, weekly) prophylactically from 2 to 4 months and analysed at 4 months, and therapeutically from 4 to 6 months and analysed at 6 months ($n = 4$ mice per group, brown signal indicated by arrowheads, nuclei counterstained with haematoxylin). Scale bar, 50 μm. Quantification of cleaved caspase-3-positive alveolar epithelial cells from the immunohistochemistry sections also shown. **i**, Western blot analysis for cleaved caspase-3 (c-Cas-3) in total lung homogenate from mice described in **h**, quantification relative to β-actin (prophylactic groups: FA $n = 7$, CS+Ig $n = 7$, CS+LTβR-Ig $n = 6$ mice per group, therapeutic groups: FA $n = 6$, CS+Ig $n = 5$, CS+LTβR-Ig $n = 6$ mice per group, pooled from two independent experiments), individual mice shown. For gel source data see Supplementary Fig. 1. **j–l**, The mouse AT2-like cell line LA4 was stimulated with LTβR-Ag (2 μg ml⁻¹), recombinant mouse TNF (1 ng ml⁻¹) or a combination of both, in the presence or absence of necrostatin-1 (Nec1, 50 μM) (**j**) and (**k**) or Z-Val-Ala-DL-Asp-fluoromethylketone (z-VAD, 20 μM) (**l**). Apoptosis was assessed at 6 h (**j–l**) and 24 h (**k, l**) by flow cytometric analysis of annexin V and propidium iodide (PI) staining ($n = 2$–3, repeated twice, pooled data shown in **k**). **m, n**, Wound-healing assay in LA4 cells grown to confluence, scratched and then incubated with LTβR-Ag (2 μg ml⁻¹), recombinant mouse TNF (1 ng ml⁻¹) or a combination of both, in the presence or absence of necrostatin-1 (50 μM). **m**, Representative images at 0 h and 56 h after scratch are shown ($n = 4$ from one experiment). Scale bar, 200 μm. **n**, Degree of wound closure (100% representing fully closed) at 56 h ($n = 4$). Data are mean ± s.d. P values determined by one-way ANOVA multiple comparisons Bonferroni test (**h, i, k, l, n**).
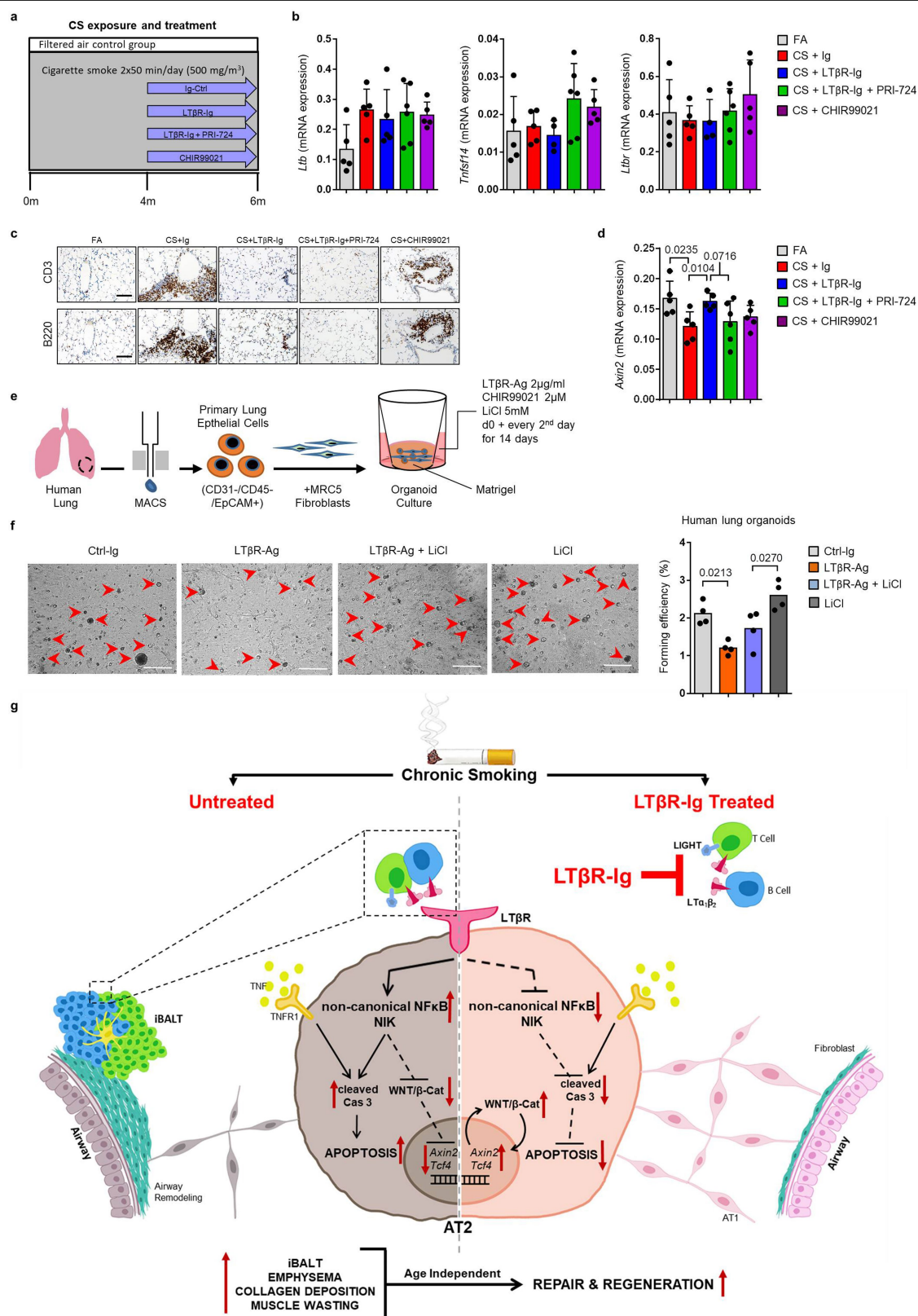
Extended Data Fig. 9 | See next page for caption.

Article

Extended Data Fig. 9 | LTβR stimulation regulates WNT/β-catenin-signalling. a, GSEA of canonical WNT signalling (GO: 0060070) and β-catenin/TCF transcription factor complex assembly (GO:1904837) in transcriptomic array data from the lungs of B6 mice after 6 months exposure to filtered air, cigarette smoke plus Ig, or cigarette smoke plus LTβR–Ig fusion protein therapeutically ($n = 3$ mice per group) and publicly available array data from lung tissue (GSE47460–GPL14550) of healthy participants ($n = 91$) versus patients with COPD ($n = 145$). **b**, Representative images of immunohistochemical analysis for AXIN2 in lung sections from healthy participants ($n = 6$) and patients with COPD ($n = 8$) (brown signal indicated by arrowheads, nuclei counterstained with haematoxylin). Scale bar, 50 μm. **c**, mRNA expression levels of *Nkd1* and *Lgr5* relative to *Hprt* in primary mouse AT2 cells treated with LTβR-Ag (2 μg ml^{-1}) for 24 h, with or without mouse rWNT3A (100 ng ml^{-1}) ($n = 5$ individual experiments). **d**, mRNA expression levels of *Tcf4* relative to *Hprt* in the LA4 cells stimulated with LTβR-Ag (2 μg ml^{-1}) or recombinant mouse TNF (1 ng ml^{-1}) ($n = 3$, repeated three times). **e**, mRNA expression levels of *Tcf4* relative to *Hprt* in LA4 cells stimulated with LTβR-Ag (2 μg ml^{-1}) plus recombinant mouse TNF (1 ng ml^{-1}) with or without necrostatin-1 (50 μM), and the IKK kinase inhibitors TPCA-1 (10 μM) or BAY 11-7082 (10 μM) ($n = 2$, repeated twice). **f**, mRNA expression levels of *AXIN2* relative to *HPRT* and normalized to vehicle, in human A549 cells treated with human LTβR-Ag (0.5 μg ml^{-1}) for 24 h with or without TPCA-1 (5 μM) ($n = 3$ independent experiments). **g**, WNT/β-catenin luciferase reporter activity in mouse MLE12 cells, activated by GSK-3β inhibitor (CHIR99021, 1 μM) and treated with LTβR-Ag at the concentrations indicated for 24 h (activity relative to CHIR alone,

$n = 2–9$). **h**, Western blot analysis for β-catenin in MLE12 cells treated with LTβR-Ag (2 μg ml^{-1}) for 24 h with or without mouse rWNT3A (100 ng ml^{-1}) plus bortezomib (10 nM). Quantification relative to actin shown ($n = 3$ independent experiments). For gel source data, see Supplementary Fig. 1. **i**, mRNA expression levels of *TCF4* relative to *HPRT* in ex vivo human precision-cut lung slices stimulated for 24 h with recombinant human TNF (20 ng ml^{-1}) or LTβR-Ag (2 μg ml^{-1}) for 24 h ($n = 5$ slices from individual lungs). **j**, Western blot analysis for β-catenin in MLE12 cells treated with mouse rWNT3A (200 ng ml^{-1}) and TNFSF14 (200 ng ml^{-1}) for 30 h. Quantification relative to vinculin shown ($n = 3$ independent experiments). For gel source data, see Supplementary Fig. 1. **k**–**m**, B6 mice were treated with a single oropharyngeal application of PBS ($n = 8$), PPE (40 U kg^{-1} body weight) ($n = 7$ mice per group) or PPE followed by LTβR–Ig fusion protein (80 μg intraperitoneally, weekly) 28 days later for 2 months and all analysed after 3 months ($n = 8$ mice per group); see Extended Data Fig. 7a. **k**, mRNA expression levels of *Axin2*, *Bcl9l*, *Cdh1*, *Dvl1*, *Gsk3b*, *Rab5a*, *Tcf4*, *Wif1*, *Wnt2* and *Wnt4* relative to *Hprt*, determined by qPCR in whole lung. **l**, Representative images of immunohistochemical analysis for TCF and AXIN2 in lung sections from the mice described ($n = 4$ mice per group, brown signal indicated by arrowheads, nuclei counterstained with haematoxylin). Scale bar, 25 μm. **m**, Quantification of alveolar epithelial cells positive for TCF4 and AXIN2 from **l**. Data shown as individual lungs (**c**, **i**) or mean ± s.d. (**d**–**h**, **j**, **k** and **m**). *P* values determined by one-tailed (**c**) or two-tailed (**i**) paired Student's *t*-test, two-tailed unpaired Student's *t*-test (**h**, **j**) or one-way ANOVA multiple comparisons Bonferroni test (**d**–**g** (compared to vehicle in **g**), **k**, **m**).

a CS exposure and treatment

Filtered air control group

Cigarette smoke 2x50 min/day (500 mg/m³)

Ig-Ctrl
LTβR-Ig
LTβR-Ig + PRI-724
CHIR99021

0m   4m   6m

b

Ltb (mRNA expression)

Tnfsf14 (mRNA expression)

Ltbr (mRNA expression)

☐ FA
☐ CS + Ig
☐ CS + LTβR-Ig
☐ CS + LTβR-Ig + PRI-724
☐ CS + CHIR99021

c

FA   CS+Ig   CS+LTβR-Ig   CS+LTβR-Ig+PRI-724   CS+CHIR99021

CD3

B220

d

Axin2 (mRNA expression)

0.0235
0.0104
0.0716

☐ FA
☐ CS + Ig
☐ CS + LTβR-Ig
☐ CS + LTβR-Ig + PRI-724
☐ CS + CHIR99021

e

Human Lung → MACS → Primary Lung Epithelial Cells (CD31-/CD45-/EpCAM+) → +MRC5 Fibroblasts → Organoid Culture

LTβR-Ag 2µg/ml
CHIR99021 2µM
LiCl 5mM
d0 + every 2nd day
for 14 days

Matrigel

f

Ctrl-Ig   LTβR-Ag   LTβR-Ag + LiCl   LiCl

Human lung organoids

Forming efficiency (%)

0.0213   0.0270

☐ Ctrl-Ig
☐ LTβR-Ag
☐ LTβR-Ag + LiCl
☐ LiCl

g

Chronic Smoking

Untreated   LTβR-Ig Treated

LIGHT   T Cell

LTβR-Ig ⊣   B Cell

LTα₁β₂

LTβR

TNF
TNFR1

non-canonical NFκB   non-canonical NFκB
NIK   NIK

cleaved Cas 3   cleaved Cas 3

WNT/β-Cat   WNT/β-Cat

APOPTOSIS   APOPTOSIS

Axin2   *Axin2*
Tcf4   *Tcf4*

AT2   AT1

Fibroblast

Airway   Airway

iBALT

Airway Remodeling

iBALT
EMPHYSEMA
COLLAGEN DEPOSITION
MUSCLE WASTING

Age Independent → REPAIR & REGENERATION ↑

Extended Data Fig. 10 | See next page for caption.

Article

nature research

Corresponding author(s):   Ali Önder Yildirim
Mathias Heikenwälder

Last updated by author(s): Jul 23, 2020

Reporting Summary

Nature Research wishes to improve the reproducibility of the work that we publish. This form provides structure for consistency and transparency in reporting. For further information on Nature Research policies, see Authors & Referees and the Editorial Policy Checklist.

Statistics

For all statistical analyses, confirm that the following items are present in the figure legend, table legend, main text, or Methods section.

n/a	Confirmed	
☐	☒	The exact sample size (*n*) for each experimental group/condition, given as a discrete number and unit of measurement
☐	☒	A statement on whether measurements were taken from distinct samples or whether the same sample was measured repeatedly
☐	☒	The statistical test(s) used AND whether they are one- or two-sided *Only common tests should be described solely by name; describe more complex techniques in the Methods section.*
☐	☒	A description of all covariates tested
☐	☒	A description of any assumptions or corrections, such as tests of normality and adjustment for multiple comparisons
☐	☒	A full description of the statistical parameters including central tendency (e.g. means) or other basic estimates (e.g. regression coefficient) AND variation (e.g. standard deviation) or associated estimates of uncertainty (e.g. confidence intervals)
☐	☒	For null hypothesis testing, the test statistic (e.g. *F*, *t*, *r*) with confidence intervals, effect sizes, degrees of freedom and *P* value noted *Give P values as exact values whenever suitable.*
☒	☐	For Bayesian analysis, information on the choice of priors and Markov chain Monte Carlo settings
☒	☐	For hierarchical and complex designs, identification of the appropriate level for tests and full reporting of outcomes
☒	☐	Estimates of effect sizes (e.g. Cohen's *d*, Pearson's *r*), indicating how they were calculated

Our web collection on statistics for biologists contains articles on many of the points above.

Software and code

Policy information about availability of computer code

Data collection	Organoids were imaged using a Cytation1 cell imaging reader running Gen5 v3.08 software (Biotek).
	Lung Function measurements were acquired using the flexiVent system running Flexiware v7.6.4 software (Scireq) and gases for diffusion capacity using a 3000 Micro GC Gas Analyser (Infinicon) running EZ IQ software v3.3.2 (Infinicon).
	Single cell RNA-sequencing was carried out using the Drop-seq pipeline v2.3.0 (https://github.com/broadinstitute/Drop-seq) and STAR (v2.5.3a) for the alignment of reads to the mm10 reference genome.
	Proteomics were generated by running trypsin digested proteins on a UltiMate 3000 UHPLC system and eluting peptides have been analyzed by an online coupled Q-Exactive-HF-X mass spectrometer running software version Exactive Series 2.9 (Thermo Fisher Scientific).
	Micro array data was obtained using Mouse Ref-8 v2.0 Expression BeadChips (Illumina) and processed using the GenomeStudioV2010.1 software (gene expression module version 1.6.0) in combination with the MouseRef-8_V2_0_R3_11278551_A.bgx annotation file.
	Flow cytometry data was acquired using FACSDiva software v6.1.3 ran on a BD FACSCanto II (apoptosis analysis) or FACSDiva software v8.0.1 ran on a BD FACSFortessa (lung tissue).
	qPCR data was obtained using a StepOnePlus™ 96 well Real-Time PCR System running StepOne software v2.3 (Applied Biosystems).
	Histology images were aquired using Zeiss Mirax Microimmaging slide scanner running MIRAXDESK v1.12.25.1 and Mirax viewer v1.12.22.0 software (Zeiss, 3D Histech).
	Multiplex immunofluorescence images were processed using FIJI and the FIJI plugin HyperStackReg V5.6 and ImageJ plugin HyperStackReg V5.6 (http://doi.org/10.5281/zenodo.2252521).
	Western blot bands were detected and quantified using the Chemidoc XRS+ system running ImageLab v5.2.1 software (Bio-Rad) or ImageJ (v1.49o).
	Luciferase activity was determined using a luminescence plate reader (Berthold Technologies) running MikroWin v4.41 (Berthold Technologies).
Data analysis	Organoids were quantified through ImageJ v1.52a software.
	Single cell RNA-sequencing downstream analysis was performed using the Scanpy package (https://github.com/theislab/Scanpy). All code

used for data visualization of the single cell RNA-Seq data can be found at https://github.com/theislab/2020_Inhibition_LTbetaR-signalling.

The MaxQuant software v1.6.12.0 (https://www.biochem.mpg.de/6304115/maxquant) was used to process proteomics data and the Perseus software package v1.6.10.50 (https://www.biochem.mpg.de/6304220/perseus) for further analysis.

CARMAweb v1.6 was used for quantile normalization and statistical analysis. CARMAweb v1.6 includes R version 3.2.3, maDB 1.10.3, limma 3.26.9 and preprocessCore 1.32.0.

Heat maps of micro array and qPCR data were generated by Genesis software (Release 1.7.7, Institute for Genomics and Bioinformatics, Graz University of Technology).

Flow cytometry data was analysed using FACSDiva v6.1.3 (apoptosis analysis), Flowlogic v7.3 and FlowJo v10.6.1 software (lung tissue analysis).

Multiplex immunofluorescence quantitation was performed using Ilastik v1.3.3post2 (www.ilastik.org) and CellProfiler v3.1.9 (https://www.nature.com/articles/nmeth.1984).

Histology data was analysed using the computer-assisted stereological toolbox software Visopharm Integrator System (VIS) v6.0.0.1765 (newCAST, Visiopharm).

AxioVision v4.9.1.0 software (Zeiss) to calculate wound surface area.

Luminescence values were analysed with WinGlow Software MikroWin v4.41 (Berthold Technologies).

GSEA software from the Broad Institute v4.0.1 was used to determine the enrichment of gene lists in microarray and proteomics data, with gene lists also obtained from Ingenuity Pathway Analysis (IPA) Spring Release 2016 (Qiagen).

Microsoft Excel v 14.0.7237.5000 (part of Microsoft Office Professional Plus 2010) for normalisation and analysis of downloaded series matrix files from the NCBI GEO databases described below.

Statistical analyses were conducted using GraphPad Prism v6.00 or v8.2.1.

For manuscripts utilizing custom algorithms or software that are central to the research but not yet described in published literature, software must be made available to editors/reviewers. We strongly encourage code deposition in a community repository (e.g. GitHub). See the Nature Research guidelines for submitting code & software for further information.

Data

Policy information about availability of data

All manuscripts must include a data availability statement. This statement should provide the following information, where applicable:
- Accession codes, unique identifiers, or web links for publicly available datasets
- A list of figures that have associated raw data
- A description of any restrictions on data availability

Microarray data was submitted to the NCBI Gene Expression Omnibus (GEO) database (https://www.ncbi.nlm.nih.gov/geo/) accession number GSE125521.

Single cell RNA-Seq data was submitted to the NCBI GEO database accession number GSE151674.

All code used for data visualization of the single cell RNA-Seq data can be found at https://github.com/theislab/2020_Inhibition_LTbetaR-signalling.

Single cell RNA-Seq metadata can be found in Supplementary Table 39.

Proteomics data can be found in Supplementary Table 40.

Series matrix files were also downloaded from the NCBI GEO databases: GSE47460-GPL14550, GSE37768, GSE56768 and GSE52509.

Proteomic peak lists were searched against the mouse Uniprot FASTA database (version November 2016) https://www.uniprot.org/proteomes/UP000000589.

All other data supporting the findings of this study are available within the paper and Supplementary Information.

Source Data for Figs. 1-4 and Extended Data Figs. 1-10 are provided with the paper.

All data are also available from the corresponding authors upon reasonable request.

Field-specific reporting

Please select the one below that is the best fit for your research. If you are not sure, read the appropriate sections before making your selection.

☒ Life sciences   ☐ Behavioural & social sciences   ☐ Ecological, evolutionary & environmental sciences

For a reference copy of the document with all sections, see nature.com/documents/nr-reporting-summary-flat.pdf

Life sciences study design

All studies must disclose on these points even when the disclosure is negative.

Sample size	No statistical methods were used to predetermine sample size. Sample sizes were chosen based upon similar studies from the literature by ourselves and others and sufficient to detect statistically significant differences between groups. Please see doi:10.15252/emmm.201708349, doi:10.1084/jem.20160675 and doi:10.1038/nm.4021. The sample sizes were adequate as the differences between experimental groups were reproducible. All sample sizes for every group can be found in the figure legends.
Data exclusions	In all experiments values measured met QC criteria (eg. effective staining or gene expression), which was predetermined, no data was excluded post analysis.
Replication	All findings were reliably reproduced, with group sizes and the number of independent repeats described in the figure legends.
Randomization	Mice were randomly assigned into experimental groups. Human lung tissue from explanted lungs of transplant patients was taken based upon a clinical diagnosis of COPD see Supplementary Table 1, for controls random unused donor lungs were collected from lungs declined for transplant after second opinion inspection because of kidney tumor, logistics or presence of microthrombi. Human lung tissue from patients who underwent lung tumor resection was used for the preparation of precision cut lung slices and slices were randomly assigned to

experimental groups. Primary human AT2 cells were isolated from fresh human lung tissue of de-identified healthy donors and randomly assigned to experimental groups. For in vitro cell culture experiments wells were randomly assigned to experimental groups.

Blinding

Quantitative morphometry on lung sections was undertaken by readers blinded to the study groups. Microarray experiments and analysis was undertaken by personnel blinded to the study groups. Blinding was not carried out for other experiments to verify that each experiment contained all groups and appropriate controls.

Reporting for specific materials, systems and methods

We require information from authors about some types of materials, experimental systems and methods used in many studies. Here, indicate whether each material, system or method listed is relevant to your study. If you are not sure if a list item applies to your research, read the appropriate section before selecting a response.

Materials & experimental systems

n/a	Involved in the study
☐	☒ Antibodies
☐	☒ Eukaryotic cell lines
☒	☐ Palaeontology
☐	☒ Animals and other organisms
☐	☒ Human research participants
☒	☐ Clinical data

Methods

n/a	Involved in the study
☒	☐ ChIP-seq
☐	☒ Flow cytometry
☒	☐ MRI-based neuroimaging

Antibodies

Antibodies used

Agonistic antibody to mouse LTβR, clone ACH6, used at 2ug/ml, kindly supplied by Jeffrey Browing (Biogen Idec)
Agonistic antibody to human LTβR, clone BS1, used at 0.5-2ug/ml, kindly supplied by Jeffrey Browing (Biogen Idec)

Immunohistochemistry:
RelA/p65, clone A, 1:500, Cat. No. sc-109, Santa Cruz
RelB, clone C-19, 1:400, Cat. No. sc-226, Santa Cruz
CD20, clone L26, 1:100, Cat. No. MSK008, Zytomed Systems
B220, clone RA3-6B2, 1:3000, Cat. No. 553084, BD Biosciences
CD3, clone SP7, 1:500, Cat. No. RBK024, Zytomed Systems
CD68, polyclonal, 1:100, Cat. No. ab125212, Abcam
Collagen I, polyclonal, 1:250, Cat. No. ab21286, Abcam
pSMAD2, polyclonal, 1:500, Cat. No. AB3849, Merck Millipore
LTB, clone B27, 1:1000, kindly supplied by Jeffrey Browing, Biogen Idec
cleaved caspase3, polyclonal, 1:300, Cat. No. 9661, Cell Signaling Technology
TCF4, polyclonal, 1:100, Cat. No. ab185736, Abcam
Axin2, polyclonal, 1:2000, Cat. No. ab32197, Abcam

Multiplex Immunofluorescence:
B220, clone RA3-6B2, 1:500, Cat. No. 103202, BioLegend
CD4, clone 4SM95, 1:200, Cat. No. 14-9766-82, ThermoFisher
CD8a, clone 4SM15, 1:200, Cat. No. 14-0808-82, ThermoFisher
IBA1, polyclonal, 1:1000, Cat. No. 100369-764, VWR
iNOS, polyclonal, 1:100, Cat. No. ab15323, Abcam
CD206, polyclonal, 1:500, Cat. No. 18704-1-AP, ProteinTech
anti-Rabbit 555, 1:500, Cat. No. 4413S, Cell Signaling
anti-Rabbit 647, 1:500, Cat. No. 4414S, Cell Signaling
anti-Rat 647, 1:500, Cat. No. 4418S, Cell Signaling

Western Blotting:
RelB, clone D7D7W, 1:1000, Cat. No. 10544, Cell Signaling
p52 (and p100), polyclonal, 1:1000, Cat. No. 4882, Cell Signaling
cleaved caspase-3, polyclonal, 1:1000, Cat. No. 9661, Cell Signaling
beta-catenin, clone 14, 1:1000, Cat. No. 610154, BD Biosciences
beta-actin, clone AC-15, 1:50000, Cat. No. A3854, Sigma-Aldrich
vinculin, clone 7F9, 1:1000, Cat. No. sc-73614, Santa Cruz
tubulin, clone B-5-1-2, 1:5000, Cat. No. T6074, Sigma-Aldrich

Flow cytometry:
CCR2-BV650, clone SA203G11, 1:100, Cat. No. 150613, BioLegend
CD103-APC, clone 2E7, 1:100, Cat. No. 121414, BioLegend
CD11b-eF450, clone M1/70, 1:400, Cat. No. 48-0112-82, Thermofisher
CD11b-BV570, clone M1/70, 1:400, Cat. No. 101233, BioLegend
CD11b-APC, clone REA592, 1:200, Cat. No. 130-113-802, Miltenyi Biotec
CD11c-PerCpCy5.5, clone N418, 1:200, Cat. No. 45-0114-82, Thermofisher
CD11c-BV510, clone HL3, 1:200, Cat. No. 562949, BD Biosciences

CD11c-AF700, clone N418, 1:200, Cat. No. 117320, BioLegend
CD127-FITC, clone a7r34, 1:200, Cat. No. 135007, BioLegend
CD19-PerCpCy5.5, clone 1D3, 1:400, Cat. No. 5511001, BD Biosciences
CD19-PE-Vio 770, clone REA749, 1:200, Cat. No. 130-112-037, Miltenyi Biotec
CD206-AF647, clone C068C2, 1:400, Cat. No. 141712, BioLegend
CD25-BV711, clone pc61, 1:200, Cat. No. 102049, BioLegend
CD4-AF700, clone RM4-5, 1:200, Cat. No. 100536, BioLegend
CD44-PE-Cy7, clone im7, 1:200, Cat. No. 103029, BioLegend
CD45-BV510, clone 30-F11, 1:200, Cat. No. 103138, BioLegend
CD45-APC-Cy7, clone 30-F11, 1:400, Cat. No. 557659, BD Biosciences
CD45-BV785, clone 30-F11, 1:800, Cat. No. 564225, BD Biosciences
CD62L-Dazzle, clone MEL-14, 1:200, Cat. No. 104448, BioLegend
CD68-APC-Cy7, clone FA-11, 1:200, Cat. No. 137024, BioLegend
CD69-PE, clone H1.2F3, 1:200, Cat. No. 104508, BioLegend
CD8-PCP-Cy5.5, clone 53-6.7, 1:200, Cat. No. 100734, BioLegend
CD86-PE, clone GL1, 1:400, Cat. No. 12-0862-83, Thermofisher
CX3CR1-BV711, clone SA011F11, 1:400, Cat. No. 149031, BioLegend
EOMES-PE-Cy7, clone dan11mag, 1:200, Cat. No. 25-4875-82, Thermofisher
F4/80-PE-Cy7, clone BM8, 1:200, Cat. No. 50-4801-80, Thermofisher
F4/80-BV650, clone BM8, 1:200, Cat. No. 123149, BioLegend
FoxP3-AF647, clone MF-14, 1:200, Cat. No. 126407, BioLegend
GL7-Pacific Blue, clone GL7, 1:100, Cat. No. 144614, BioLegend
IgG-FITC, Poly4053, 1:100, Cat. No. 405305, BioLegend
Ki67-BV421, clone sola15, 1:500, Cat. No. 48-5698-80, eBioscience
Ly6C-AF488, clone HK1.4, 1:400, Cat. No. 128021, BioLegend
Ly6G-AF700, clone 1A8, 1:400, Cat. No. 561236, BD Biosciences
MerTK-BV480, clone 108928, 1:200, Cat. No. 747896, BD Biosciences
MHC II-FITC, clone M5/114.15.2, 1:400, Cat. No. 107606, Biolegend
MHC II-PerCP-Vio700, clone REA813, 1:200, Cat. No. 130-112-391, Miltenyi Biotec
NK1.1-BV711, clone PK136, 1:200, Cat. No. 108745, BioLegend
NK1.1-PE, clone PK136, 1:400, Cat. No. 553165, BD Biosciences
NKp46-Dazzle, clone 29A1.4, 1:200, Cat. No. 137630, BioLegend
PD-1-BV605, clone 29f.1a12, 1:200, Cat. No. 135220, BioLegend
PD-L1-BV711, clone MIH5, 1:400, Cat. No. 563369, BD Biosciences
Siglec-F-BV421, clone E50-2440, 1:200, Cat. No. 565934, BD Biosciences
Tbet-BV421, clone 4b10, 1:200, Cat. No. 644832, BioLegend
TCF1-FITC, clone C63D9, 1:200, Cat. No. 6444S, Cell Signaling
TCRbeta-BV650, clone H57-597, 1:200, Cat. No. 742483, BD Biosciences
TCRbeta-PE-Cy7, clone H57-597, 1:400, Cat. No. 25-5961-82, Thermofisher
Tim3-APC, clone RMT3-23, 1:200, Cat. No. 119706, BioLegend

| Validation | Antibodies were titred out based on recommendations by the respective manufactures. Validation of commercial antibodies was undertaken on a regular quality control of each lot by the manufacturer (e.g. Biolegend "Each lot of this antibody is quality control tested by immunofluorescent staining with flow cytometric analysis." |

For validation of the agonistic anti-LTβR antibodies clone BS1 and ACH6 supplied by Jeffrey Browing (Biogen Idec) please see the following publications: PMID: 23349015 and PMID: 17018619
For validation of anti-LTB, clone B27, supplied by Jeffrey Browing (Biogen Idec) used in immunohistochemistry please see: PMID: 26398497.

Validation of commercial antibodies please see:
Immunohistochemistry
RelA/p65, clone A, Cat. No. sc-109, Santa Cruz, PMID: 29287688 and PMID: 27793764
RelB, clone C-19, Cat. No. sc-226, Santa Cruz, PMID: 27217485 and PMID: 26042424
CD20, clone L26, Cat. No. MSK008, Zytomed Systems, PMID: 3881477 and PMID: 6376628
B220, clone RA3-6B2, Cat. No. 553084, BD Biosciences, PMID: 29793924
CD3, clone SP7, Cat. No. RBK024, Zytomed Systems, PMID: 9023553 and PMID: 2553046
CD68, Cat. No. ab125212, Abcam, PMID: 31774937 and PMID: 31782624
Collagen I, Cat. No. ab21286, Abcam, PMID: 31940494 and PMID: 31166803
pSMAD2, Cat. No. AB3849, Merck Millipore, PMID: 31609088 and PMID: 28806779
cleaved caspase3, Cat. No. 9661, Cell Signaling Technology, PMID: 32096822 and PMID: 32060280
TCF4, Cat. No. ab185736, Abcam, PMID: 30930294 and PMID: 28627514
Axin2, polyclonal, 1:2000, Cat. No. ab32197, Abcam, PMID: 31488864 and PMID: 25383518

Multiplex Immunofluorescence
B220, clone RA3-6B2, Cat. No. 103202, BioLegend, PMID: 15314695, 17529982, 20512127
CD4, clone 4SM95, Cat. No. 14-9766-82, ThermoFisher, PMID: 26847386, 29186654
CD8a, clone 4SM15, Cat. No. 14-0808-82, ThermoFisher, PMID: 27656328
IBA1, Cat. No. 100369-764, VWR, PMID: 32607882
iNOS, Cat. No. ab15323, Abcam, PMID: 31426846
CD206, Cat. No. 18704-1-AP, ProteinTech, PMID: 27845069, 23482450
anti-Rabbit 555, Cat. No. 4413S, Cell Signaling, PMID: 28165507
anti-Rabbit 647, Cat. No. 4414S, Cell Signaling, PMID: 27430169
anti-Rat 647, Cat. No. 4418S, Cell Signaling, PMID: 25392531

Western Blotting
RelB, clone D7D7W, Cat. No. 10544, Cell Signaling, PMID: 31125342 and PMID: 30301887
p52 (and p100), Cat. No. 4882, Cell Signaling, PMID: 30737385 and PMID: 30250175
cleaved caspase-3, Cat. No. 9661, Cell Signaling, PMID: 31873117 and PMID: 31601814
beta-catenin, clone 14, Cat. No. 610154, BD Biosciences, PMID: 30808932 and PMID: 26935695
beta-actin, clone AC-15, Cat. No. A3854, Sigma-Aldrich, PMID: 31449520 and PMID: 30420655
vinculin, clone 7F9, Cat. No. sc-73614, Santa Cruz, PMID: 31253783 and PMID: 26442967
tubulin, clone B-5-1-2, Cat. No. T6074, Sigma-Aldrich, PMID: 31399584 and PMID: 30446640

Flow cytometry:
CCR2-BV650, clone SA203G11, Cat. No. 150613, BioLegend, PMID: 30998796
CD103-APC, clone 2E7, Cat. No. 121414, BioLegend, PMID: 29166591 and PMID: 29942093
CD11b-eF450, clone M1/70, Cat. No. 48-0112-82, Thermofisher, PMID: 30936549
CD11b-BV570, clone M1/70, Cat. No. 101233, BioLegend, PMID: PMID: 30245008
CD11b-APC, clone REA592, Cat. No. 130-113-802, Miltenyi Biotec, PMID: 32195341
CD11c-PerCpCy5.5, clone N418, Cat. No. 45-0114-82, Thermofisher, PMID: 29429633
CD11c-BV510, clone HL3, Cat. No. 562949, BD Biosciences, PMID: 30936549
CD11c-AF700, clone N418, Cat. No. 117320, BioLegend, PMID: 30833511 and PMID: 27417580
CD127-FITC, clone a7r34, Cat. No. 135007, BioLegend, PMID: 26768662
CD19-PerCpCy5.5, clone 1D3, Cat. No. 5511001, BD Biosciences, PMID: 11120817
CD206-AF647, clone C068C2, Cat. No. 141712, BioLegend, PMID: 30936549 and PMID: 31375662
CD25-BV711, clone pc61, Cat. No. 102049, BioLegend, PMID: 32358491 and PMID: 30540940
CD4-AF700, clone RM4-5, Cat. No. 100536, BioLegend, PMID: 31350404 and PMID: 29045902
CD44-PE-Cy7, clone im7, Cat. No. 103029, BioLegend, PMID: 30936549 and PMID: 30455690
CD45-BV510, clone 30-F11, Cat. No. 103138, BioLegend, PMID: 31073183 and PMID: 30076102
CD45-APC-Cy7, clone 30-F11, Cat. No. 557659, BD Biosciences, PMID: 30936549 and PMID: 30770807
CD45-BV785, clone 30-F11, Cat. No. 564225, BD Biosciences, PMID: 30936549 and PMID: 29909986
CD62L-Dazzle, clone MEL-14, Cat. No. 104448, BioLegend, PMID: 30936549
CD68-APC-Cy7, clone FA-11, Cat. No. 137024, BioLegend, PMID: 22403066
CD69-PE, clone H1.2F3, Cat. No. 104508, BioLegend, PMID: 30936549 and PMID: 29431745
CD8-PCP-Cy5.5, clone 53-6.7, Cat. No. 100734, BioLegend, PMID: 30936549 and PMID: 29942093
CD86-PE, clone GL1, Cat. No. 12-0862-83, Thermofisher, PMID: 30936549
CX3CR1-BV711, clone SA011F11, Cat. No. 149031, BioLegend, PMID: 30936549 and PMID: 29548673
EOMES-PE-Cy7, clone dan11mag, Cat. No. 25-4875-82, Thermofisher, PMID: 30451838 and PMID: 28844693
F4/80-PE-Cy7, clone BM8, Cat. No. 50-4801-80, Thermofisher, PMID: 30936549
F4/80-BV650, clone BM8, Cat. No. 123149, BioLegend, PMID: 30936549 and PMID: 31511510
FoxP3-AF647, clone MF-14, Cat. No. 126407, BioLegend, PMID: 27117228 and PMID: 28810147
GL7-Pacific Blue, clone GL7, Cat. No. 144614, BioLegend, PMID: 31204070 and PMID: 30231983
IgG-FITC, Poly4053, Cat. No. 405305, BioLegend, PMID: 31604929 and PMID: 24747745
Ki67-BV421, clone sola15, Cat. No. 48-5698-80, eBioscience, PMID: 28123877 and PMID: 29934585
Ly6C-AF488, clone HK1.4, Cat. No. 128021, BioLegend, PMID: 31086348 and PMID: 29867149
Ly6G-AF700, clone 1A8, Cat. No. 561236, BD Biosciences, PMID: 30936549 and PMID: 30224810
MerTK-BV480, clone 108928, Cat. No. 747896, BD Biosciences, PMID: 24553136
MHC II-FITC, clone M5/114.15.2, Cat. No. 107606, Biolegend, PMID: 30936549 and PMID: 28008921
NK1.1-BV711, clone PK136, Cat. No. 108745, BioLegend, PMID: 30232272 and PMID: 28930659
NK1.1-PE, clone PK136, Cat. No. 553165, BD Biosciences, PMID: 30936549 and PMID: 30710528
NKp46-Dazzle, clone 29A1.4, Cat. No. 137630, BioLegend, PMID: 21300822
PD-1-BV605, clone 29f.1a12, Cat. No. 135220, BioLegend, PMID: 29963060 and PMID: 28898698
PD-L1-BV711, clone MIH5, Cat. No. 563369, BD Biosciences, PMID: 11238124 and PMID: 16314434
Siglec-F-BV421, clone E50-2440, Cat. No. 565934, BD Biosciences, PMID: 11579105 and PMID: 28928446
Tbet-BV421, clone 4b10, Cat. No. 644832, BioLegend, PMID: 27693353 and PMID: 30770246
TCF1-FITC, clone C63D9, Cat. No. 6444S, Cell Signaling, PMID: 28973925
TCRbeta-BV650, clone H57-597, Cat. No. 742483, BD Biosciences, PMID: 29249358 and PMID: 29136506
TCRbeta-PE-Cy7, clone H57-597, Cat. No. 25-5961-82, Thermofisher, PMID: 29249358 and PMID: 29136506
Tim3-APC, clone RMT3-23, Cat. No. 119706, BioLegend, PMID: 30469401

Eukaryotic cell lines

Policy information about cell lines

Cell line source(s)	A549, #CCL-185, ATCC LA4, #CCL-196, ATCC MLE12, #CRL-2110, ATCC MRC-5, #CCL-171, ATCC
Authentication	The cell lines were not authenticated.
Mycoplasma contamination	All cell lines were routinely tested, and tested negative for Mycoplasma.
Commonly misidentified lines (See ICLAC register)	No commonly misidentified cell lines used in the study.

Animals and other organisms

Policy information about [studies involving animals](#); [ARRIVE guidelines](#) recommended for reporting animal research

Laboratory animals	8 to 10 week and 12 month old pathogen-free female C57BL/6 mice were obtained from Charles River (Sulzfeld, Germany) and housed in rooms maintained at a constant temperature of 20-24°C and 45-65% humidity with a 12 hour light cycle. Animals were allowed food and water ad libitum.
Wild animals	No wild animals were used in the study.
Field-collected samples	No field-collected samples were used in the study.
Ethics oversight	All animal experiments were approved by the ethics committee for animal welfare of the local government for the administrative region of Upper Bavaria (Regierungspräsidium Oberbayern) and were conducted under strict governmental and international guidelines in accordance with EU Directive 2010/63/EU.

Note that full information on the approval of the study protocol must also be provided in the manuscript.

Human research participants

Policy information about [studies involving human research participants](#)

Population characteristics	Lung core samples from explanted lungs of COPD patients undergoing lung transplantation were used. Patient demographics are highlighted in Supplementary Table 36. For controls, unused donor lungs were collected. Lungs were declined for various reasons (kidney tumor, logistics, presence of microthrombi). Tumor-free tissue from six patients who underwent lung tumor resection was used for the preparation of precision cut lung slices (PCLS). Fresh human lung tissue for the generation of lung organoids was obtained from de-identified healthy donors through National Jewish hospital Human Lung Tissue Consortium (HLTC).
Recruitment	Human lung tissue from explanted lungs of transplant patients was taken based upon a clinical diagnosis of COPD from patients who underwent lung transplantation at University Hospitals (Leuven, Belgium). For controls random unused donor lungs were collected from lungs declined for transplant after second opinion inspection at University Hospitals (Leuven, Belgium). The Asklepios Biobank (Gauting, Germany) provided lung tissue from patients who underwent lung tumor resection, following informed written consent. Participants were recruited randomly. The HLTC obtains fresh lungs from Donor Alliance, our local organ procurement agency and the International Institute for the Advancement of Medicine.
Ethics oversight	Lung core samples were used following ethical approval of the University of Leuven Institutional Review Board (ML6385). Unused donor lungs were collected under existing Belgian law which allows the use of declined donor lungs for research after second opinion inspection. Tissue for PCLS was provided by the Asklepios Biobank for Lung Diseases (Gauting, Germany (project number 333-10)). All participants provided informed written consent, and the use of human tissue approved by the ethics committee of the Ludwig-Maximillian University (Munich, Germany (project number 455-12)). Lung tissue obtained from HLTC for the generation of lung organoids was used following ethical approval by the Institutional Review Board of the University of Colorado and National Jewish Hospital under IRB exempt HS-2598.

Note that full information on the approval of the study protocol must also be provided in the manuscript.

Flow Cytometry

Plots

Confirm that:

☒ The axis labels state the marker and fluorochrome used (e.g. CD4-FITC).

☒ The axis scales are clearly visible. Include numbers along axes only for bottom left plot of group (a 'group' is an analysis of identical markers).

☒ All plots are contour plots with outliers or pseudocolor plots.

☒ A numerical value for number of cells or percentage (with statistics) is provided.

Methodology

Sample preparation	Apoptosis analysis: LA4 cells were trypsinised, washed in PBS and then apotosis levels analysed using the Annexin V Apoptosis Detection Kit APC (eBioscience, ThermoFisher Scientific).

Lung analysis:
Single cell suspension was derived by using MACS Dissociator (Miltenyi Biotec, Bergisch Gladbach, Germany) according to manufacturer`s instructions. Staining was performed using Live/Dead discrimination by ZombieDyeNIR according to the manufacturer´s instructions for lymphocytes and Live/Dead discrimination by fixable viability stain FVS620 (BD) for myeloid cells. After washing (~400g, 5min, 4°C), cells were stained in 25µl of titrated antibody master mix for 20min protected from light at 4°C and washed again.

Instrument

Apoptosis analysis:
BD FACSCanto II flow cytometer (BD Biosciences)

Lung analysis:
Cells were analyzed using BD FACSFortessa (BD Biosciences)

Software

Apoptosis analysis:
BD FACSDiva v6.1.3 software.

Lung analysis:
Data was obtained using BD FACSDiva v8.0.1 and analyzed using Flowlogic v7.3 and FlowJo v10.6.1.

Cell population abundance

Absolute quantification by using CountBright™ Absolute Counting Beads.

Gating strategy

Apoptosis analysis:
Cells were gated based on size (FSC v SSC) and then analysed for AnnexinV and PI positivity.

Lung analysis:
For tSNE representation myeloid cells were downsampled to 3000 live CD45+CD11b+ and/or CD11c+ cells; and lymphocytes were downsampled to 5000 live CD45+ cells.

☒ Tick this box to confirm that a figure exemplifying the gating strategy is provided in the Supplementary Information.